Distinct waves of ovarian follicles contribute to mouse oocyte production

Qi Yin[1] and Allan C. Spradling[1,*]

[1]Howard Hughes Medical Institute and Department of Biosphere Sciences, Carnegie Institution for Science, Baltimore, MD 21218, USA

[*] corresponding author and lead contact: spradling@carnegiescience.edu

Competing interests: The authors declare that no competing interests exist.

ABSTRACT

The earliest growing mouse follicles, wave 1, rapidly develop in the ovarian medulla, while the great majority, wave 2, are stored for later use as resting primordial follicles in the cortex. Wave 1 follicles are known to mostly undergo atresia, a fate sometimes associated with the persistence of steroidogenic theca cells, but this connection is poorly understood. We characterized wave 1 follicle biology using tissue clearing, lineage tracing and scRNAseq to clarify their contributions to offspring and to steroidogenesis. Wave 1 follicles lineage marked by E16.5 *FoxL2* expression in granulosa cells, reach preantral stages containing theca cell layers by 2 weeks. Atresia begins about a week later, during which 80-100% of wave 1 follicles degrade their oocytes, turn over most granulosa cells, but retain theca cells which expand in number together with interstitial gland cells in the medulla. During puberty (5 weeks), these cells ultrastructurally resemble steroidogenic cells and highly express androgen biosynthetic genes. Unexpectedly, the *FoxL2* lineage tag also marked about 400 primordial follicles, located near the medullar-cortical boundary, that become the earliest-activated wave 2 follicles. These "boundary" or "wave 1.5" follicles generate 70-100% of the earliest mature oocytes, while fewer than 26 wave 1 follicles with oocytes survive. Consistent with their largely distinct fates in steroid or oocyte production, granulosa cells of antral wave 1 and wave 2 follicles differentially express multiple genes, including *Wnt4* and *Igfbp5*.

SIGNIFICANCE STATEMENT

We studied the ovaries of juvenile mice 2-6 weeks (wk) of age using transcriptomics and cell lineage to characterize the earliest developing groups of follicles. Wave 1 follicles begin growing at birth in the ovarian medulla, but few produce mature oocytes. Instead, most undergo partial atresia and expand steroidogenic cells expressing androgenic genes at puberty. A newly identified primordial follicle subset located at the medulla-cortex boundary are the earliest to activate and grow. Their oocytes give rise to most early offspring, while no more than a few derive from surviving wave 1 follicles. Our results highlight the importance of spatially localized follicle subgroups and show that follicular waves aid reproduction in distinct ways, some of which involve substantial atresia and cellular remodeling.

INTRODUCTION

Gametes often begin development in subgroups known as "waves" that arise at specific times and gonadal locations (Hirshfield, 1992; Hirshfield and DeSanti, 1995; Gougeon, 1996; Jiménez, 2009; DeFalco and Capel, 2009; Zheng et al., 2014a, b). In mice, the earliest developing follicles, a small group known as "wave 1", become growing primary follicles in the ovarian medulla by the time of birth without entering dormancy as primordial follicles. The remaining ~90%, "wave 2", enter quiescence before postnatal day 5 (P5) by forming primordial follicles within the ovarian cortex to support lifelong fertility (reviews: Edson et al., 2009; McKey et al., 2022) (Figure 1A). In the medulla, wave 1 follicles retain early arising bipotential granulosa cells (BPGs), which express *Foxl2* and *Nr5a2* beginning during early fetal development. In contrast, wave 2 follicles in the cortex acquire epithelial granulosa cells (EPGs), express *Foxl2* only after birth, and most express little *Nr5a2* as primordial follicles (Mork et al., 2012; Zheng et al., 2014a; Niu and Spradling, 2020; Meinsohn et al., 2021a). However, a small subset of non-growing primordial follicles was identified that did express *Nr5a2* and were proposed to be primed for activation (Meinsohn et al., 2021b).

Once primordial follicles are signaled to grow, their granulosa cells (GCs) start to proliferate and soon form multiple GC layers surrounding the oocyte (Habara et al., 2021). Granulosa cells in secondary follicles send signals encoded by Desert hedgehog (*Dhh*) and Indian hedgehog (*Ihh*) that attract ovarian mesodermal precursors to form outer theca cell layers on follicles and to synthesize steroid hormones (Liu et al., 2015). Additionally, ovarian medullary precursors generate thecal fibroblastic cells and perivascular smooth muscle cells that vascularize the thecal region and enable such follicles to collectively serve as a major systemic steroid hormone source (Guzmán et al., 2023). An ovarian cell type closely related to theca cells,

interstitial gland cells, also coordinately form in mice and many other mammals (Jiménez, 2009; Miyabayashi et al., 2015). *Nr5a2* promotes theca cell vascularization that is essential for ovulation (Duggavathi et al., 2008; Bianco et al., 2019; Guzmán et al., 2022). Two classes of steroid hormone-producing Leydig cells, fetal and adult, also arise during testis development (Miyabayashi et al., 2015; Liu et al., 2016).

Follicular cells synthesize specific steroid hormones during their development (Edson et al., 2009; Richards et al., 2017; Niu and Spradling, 2020; Meinsohn et al., 2021a). Thecal steroidogenic cells of late secondary and preantral follicles convert cholesterol to androgens through a series of enzymatic reactions involving steroidogenic acute regulatory protein (StAR), cytochrome P450 family 11 subfamily A member 1 (CYP11A1), hydroxy-delta-5-steroid dehydrogenase, 3 beta- and steroid delta-isomerase 1 (HSD3B1), cytochrome P450 family 17 subfamily A member 1 (CYP17A1), and steroid 5 alpha-reductase 1 (SRD5A1). *Cyp17a1-iCre* (*Cyp17a1* promoter driving codon-improved *Cre*) has been developed and used to label theca cells, the interstitial gland, and some granulosa cells (Bridges et al., 2008). Ovarian androgen production by theca cells during juvenile development is essential for normal maturation and puberty onset (Galas et al., 2012; Walters et al., 2019; Kelava et al., 2022). In addition, thecal androgens diffuse into neighboring GCs, where they are converted into estrogen by the action of hydroxysteroid 17-beta dehydrogenase 1 (HSD17B1) and cytochrome P450 family 19 subfamily A member 1 (CYP19A1). Estrogen produced in this manner signals the hypothalamus to initiate gonadotropin production and is essential for subsequent follicular maturation. After ovulation, the oocyte-free follicle is further modified into a corpus luteum, and its remaining granulosa cells and theca cells undergo luteinization to generate progesterone.

134 The development and function of wave 1 follicles has remained controversial. Most wave
135 1 follicles undergo atresia after reaching early antral stages (Byskov et al., 1974; Erickson et al.,
136 1985) during juvenile development (Figure 1B). This suggested they do not primarily serve a
137 direct reproductive function (Hirshfield, 1992; Hsueh et al., 1994; Eppig and Handel, 2012),
138 although these follicles are capable of developing into functional oocytes following
139 superovulation (Lamas et al., 2021) and could support fertility in an irradiated rat model (Guigon
140 et al., 2003). Theca cells of atretic follicles often survive and persist in the ovary (Erickson et al.,
141 1985; Magoffin, 2005), suggesting a function in steroid production. However, when *Foxl2-*
142 *CreERT2* was used to lineage label the granulosa cells of wave 1 follicles, marked follicles
143 substantially contributed to offspring during the initial months of fertility (Zheng et al., 2014b).

144 Here we studied wave 1 follicle development and gene expression in detail to gain deeper
145 insights into follicular waves. We found that lineage labeling using *Foxl2-CreERT2* activated in
146 early fetal stages is not specific for wave 1 follicles. Granulosa cells in about 400 primordial
147 follicles are also marked near the medulla-cortex boundary in 2week old mice, hence we termed
148 them "boundary" or "wave 1.5" follicles. Marked boundary follicles produce more than 70% of
149 early fertile oocytes, while no more than 26 intact wave 1 follicles survive to puberty. Boundary
150 follicles probably correspond to the resting primordial follicle population expressing *Nr5a2*
151 described by Meinsohn et al. (2021a, b). Thus, most of the *FoxL2-CreERT2* labeled follicles
152 contributing to offspring observed by Zheng et al. 2014a likely derived from boundary follicles
153 rather than wave 1 follicles.

154 Ovarian developmental and gene expression studies during 2-6 wks provided molecular
155 insight into gamete waves and follicular atresia. Wave 1 follicular oocytes and granulosa cells
156 mostly turn over beginning at about 3 wk. However, their theca cells increase in number and join

157 interstitial gland cells to form by puberty a mass of active steroidogenic medullar cells that retain
158 morphological evidence of their origin from atretic follicles. These steroidogenic cells highly
159 express androgenic genes when granulosa cells are still reduced in number by atresia. The
160 granulosa cell gene expression in developing wave 2 follicles also shows differences from that of
161 wave 1 follicles, indicating that the distinct developmental fates of wave 1 and wave 2 follicles
162 may depend on intrinsic gene expression differences in addition to differing levels of
163 gonadotropins.

164

165 RESULTS

166 **Wave 1 follicle development**

167 Advances that allow tissue clearing (Faire et al., 2015; Feng et al., 2017; Fiorentino et al.,
168 2020; McKey et al., 2022), now make it possible to image an entire mouse ovary without
169 sectioning. To better understand follicle waves, we employed whole mount staining combined
170 with clearing-enhanced 3D (Ce3D) method to analyze wild type C57BL/6J ovaries at the cellular
171 level (Li et al., 2017). Multiple ovaries were reconstructed during weeks (wk) 1-5 of
172 development (Table S1). In C57BL/6J mice, puberty typically occurs between 4 and 5 wk of age,
173 but the first ovulation, which signals sexual maturity, doesn't take place until 7 wk (Figure 1B)
174 (Hogan et al., 1994; Nelson et al., 1990; Zhou et al., 2007).

175 These studies allowed the number of wave 1 and wave 2 follicles to be accurately
176 determined. Wave 1 follicles begin to grow into primary follicles around the time of birth (Figure
177 S1A, B), as confirmed by gene expression analysis (Niu and Spradling, 2020). Following whole-
178 ovary imaging using a confocal microscope, the samples were analyzed using Imaris software.
179 Since nearly all oocytes are enclosed by granulosa cells by P5, it becomes feasible to accurately

180 quantify the number of follicles. At P5 and P10, we counted approximately 3,822 and 3,304 total
181 follicles, respectively (Figure 1C, D), and 278 and 293 wave 1 follicles (Figure 1E, F). Despite
182 variations in total follicle numbers among samples of the same age, the number of wave 1
183 follicles remained relatively consistent.

184 By 2 wk, wave 1 follicles in the medulla had developed into secondary follicles
185 containing 2-4 layers of granulosa cells and 1–2 layers of theca cells (Figure S1C). At 3 wk,
186 some follicles further developed into antral follicles with multiple granulosa cell layers, within
187 which granulosa cell apoptosis was observed (Figure S1D). Using the Imaris software surface
188 modeling, we quantified oocyte volume from 1 wk to 3 wk and observed a significant increase
189 during this period (Figure 1G, H).

190 **Wave 1 follicles undergo partial atresia with theca cell survival**

191 Starting around 3 wk, rather than continuing to develop, wave 1 follicles begin to
192 undergo atresia (Table S1; Supplemental Movies). We investigated the kinetics, cell specificity
193 and completeness of cellular turnover from 3 wk to 5 wk. Atretic follicles initially showed oocyte
194 distortion followed by loss, initially leaving behind disorganized granulosa within the basement
195 membrane but without affecting the theca cell layers (Figure 1I). Atretic follicles progressively
196 decreased in size and developed a cavity beneath the granulosa layer where the oocyte had
197 previously resided. Oocyte loss from wave 1 follicles increased significantly between 3 and 4
198 wk, exceeding 80% by 5 wk. (Figure 1J). Electron microscopy revealed that during atresia, as
199 oocytes degenerate, microvilli from both oocytes and granulosa cells retract from the zona
200 pellucida (ZP). The shrinking of the cavity is marked by folding of the ZP, and in atretic follicles,
201 remnants of the ZP appear to prevent further collapse of the cavity structure (Figure S2A). ZP
202 remnants in the follicular cavity have previously been used as a morphological indicator of

203 atretic follicles (Myers et al., 2004). We confirmed that these events also occur in the DBA/2J
204 strain, where atretic follicles are also first observed around 3 wk. By 7 wk, corpora lutea from
205 ovulated oocytes and cavities left behind by wave 1 oocyte loss were evident (Figure S2B). Thus,
206 by combining whole mount staining with Ce3D clearing method, we found that the great
207 majority of wave 1 follicles lose their oocytes prior to puberty and do not contribute to early
208 ovulation.

209 The loss of oocytes from most wave 1 follicles is not simply due to atresia of follicles
210 whose oocytes are defective, as superovulation at these stages can rescue many of them (Lamas
211 et al., 2021). Etymologically, atresia originates from the Greek "a-" (meaning "no") and "tresis"
212 (meaning "perforation"), referring to the absence or closure of an opening, or cavity. Atresia is
213 sometimes used simply to describe the complete turnover of follicles, which was not observed
214 for wave 1 follicles. We prefer the terms 'partial atresia' or 'remodeled follicles' to emphasize the
215 potential function of those structures that remain (Hsueh et al., 1994).

216 To analyze the cell specificity of wave 1 partial atresia, we exploited *Foxl2-CreERT2*
217 mouse line and *R26R-LSL-EYFP* reporter line to selectively lineage label GCs associated with
218 wave 1 follicles (Figure 2A). Similar genetic models have previously been used to study wave 1
219 follicle development and the duration of their fertility contribution based on tissue sections
220 (Mork et al., 2012; Zheng et al., 2014a). Following brief administration of Tamoxifen (TAM) at
221 embryonic day 16.5 (E16.5), we observed a distinct labeling pattern along the medulla–cortex
222 boundary. Most wave 1 follicles in the medulla showed mosaic EYFP-labeling of GCs at 2 wk
223 (due to the incomplete efficiency of cre-lox recombination) while GCs in the largely cortical
224 wave two follicles remained unlabeled (Figure 2B, C). On average, 201 preantral wave 1
225 derivatives—representing approximately 90% of wave 1 follicles—exhibited mosaic labeling in

226 granulosa cells (Figure 2E, F). By 5 wk, after extensive wave 1 atresia and remodeling, an
227 average of only 26 antral follicles containing healthy oocytes and EYFP-mosaic GC layers were
228 observed, approximately 70% of all antral follicles (Figure 2D-F).

229 By comparing the number of labeled GCs in healthy follicles at 3 wk with those in
230 remodeled follicles at 5 wk, we found that remodeled follicles lost not only oocytes but also 94%
231 of their GCs (Figure 2G). The remaining GCs were located adjacent to the cavity left by the
232 oocyte and approximately 80% of remodeled follicles stilled contained labeled GCs (Figure 2H).
233 To ask whether these remnant GCs remained active, lineage labeling was carried out at 5 wk and
234 analyzed one week later. The results showed that many GCs in remodeled follicles still remain
235 intact adjacent to holes left by oocytes and express *Foxl2* (Figure 2I). The turnover of wave 1
236 follicles was also observed using a different reporter mouse line *R26R-LSL-tdTomato* (Figure
237 S3A-C).

238 **Identification of an early activating subpopulation of primordial follicles**

239 Because only about 26 normal-appearing wave 1 follicles with oocytes survived even to 5
240 wk, which seemed too few to support the months of early fertility ascribed to wave 1 by previous
241 reports (Zheng et al., 2014a), we looked for follicles other than wave 1 that might be also labeled
242 by *Foxl2* expression. We observed that *Foxl2-CreERT2* activated by TAM injection at E16.5 in 2
243 wk juvenile ovaries also labels a subset of primordial follicles located near the medulla-cortex
244 boundary (Figures 3A). A mean of 421 labeled "boundary" follicles mosaic for 1-4 EYFP-
245 positive GCs were identified among 5,843 total follicles (7%) (Figure 3B). Because only 1-4
246 GCs where labeled from among an average of 8 GCs (Chen et al., 2022), some additional
247 boundary follicles were likely missed for stochastic reasons due to the low efficiency of cre-lox

248 recombination. Applying the Poisson distribution based on the relative proportion of follicles
249 with 1 or 2 labeled GCs, suggested that 90% of boundary follicles were detected.

250 Because of the biological interest of this subgroup of primordial follicles, we repeated
251 activation of *Foxl2-CreERT2* at E16.5 in a separate experiment with a different reporter line,
252 *R26R-LSL-tdTomato.* The results confirmed the existence and properties of boundary follicles
253 (Figure S3A-D). Boundary follicles also identified following TAM injection at E14.5 although at
254 a lower frequency (Figure 3C). Thus, the existence of this subclass was confirmed in multiple
255 experiments.

256 Primordial follicles begin to activate after 2wk (Zheng et al. 2014a). If boundary follicles
257 behave like other primordial follicles, we would expect subsequently only 7% of recently
258 activated wave 2 growing follicles would show EYFP mosaic GCs at later times. Instead, we
259 found that among secondary follicles at 5 wk, nearly 70% contained EYFP-positive GCs (Figure
260 3D), indicating that boundary follicles activate at the time of the earliest known primordial
261 follicles, and rise from 7% of quiescent to >70% of early activating follicles imply they comprise
262 most of the earliest activated primordial follicles. Moreover, they correspond in location and
263 properties to the inactive but poised primordial follicles described by Meinsohn et al. (2021a, b).

264 **Partial atresia of wave 1 follicles does not affect theca cells which expand in number**

265 We then used lineage labeling to investigate the fate of wave 1 theca cells after the onset
266 of atresia. *Cyp17a1* is an essential gene involved in steroidogenesis and is expressed in the
267 steroidogenic theca cells (STCs) and interstitial gland cells (IGCs). We validated that theca cells
268 strongly express the steroid biosynthetic enzyme CYP17A1 from 3 wk to 5 wk using
269 immunofluorescent staining (Figure S4A). To label STCs, we crossed the *Cyp17a1-icre*
270 transgenic mouse line with the *R26R-LSL-tdTomato* reporter line (Figure 4A). In 2 wk ovaries,

271 tdTomato expression was observed in theca cells sheathing large medullar follicles (Figure 4B;
272 arrowhead). Additional cells intertwined with theca cells, which appear to be IGCs (Figure 4B;
273 boxed region), were visualized using Imaris and pseudo-colored using the surface model to
274 highlight their structure (Figure 4C). A relatively small number of GCs also become labeled
275 initially (Figure S4B, arrowheads), possibly because GC precursor cells briefly express *Cyp17a1*
276 during embryonic stages (Mawaribuchi et al., 2014).

277 Between 2 wk to 5 wk, the number of tdTomato-labeled cells associated with nuclear
278 cavities dramatically increases as wave 1 follicle atresia and remodeling proceeds to involve
279 more such follicles (Figure 4D, E). Because over 90% of GCs turn over as part of wave 1
280 remodeling (Figure 2G), the tdTomato-positive cells associated with remodeled wave 1 follicles
281 by 5 wk mostly represent abundant STCs and IGCs. Oil red O staining documented abundant
282 lipid droplet accumulation in these cells from 2 wk to 5 wk (Figure 4F, G). Antibody staining
283 revealed abundant expression of the steroidogenic enzyme HSD3B1 and the lipid storage protein
284 PLIN1 in these cells, which are located in the medulla (Figure 4H). Electron microscopy
285 confirmed that expanded wave 1 follicular cells display distinctive lipid droplets and
286 mitochondria characteristic of STCs and IGCs (Figure 4I, S4C). Using Imaris software surface
287 model, we reconstructed labeled STCs and IGCs throughout the entire ovary. By 5 wk, atretic
288 wave 1 follicles had generated a cellular cluster within the medulla that was dominated by
289 expanded numbers of steroidogenic cells (Figure 4J). This structure persists within the ovary at
290 least until 7 wk (Figure S4D).

291 **Mapping cell transcription during wave 1 remodeling**

292 To gain further insight into wave 1 follicle development and remodeling, we analyzed
293 gene expression in single cells from ovaries every wk from wk2 to wk6, covering pre- and peri-

294 pubertal stages (Figure 5A; Supplemental Datasets S1-S6). A total of 31 initial clusters (c0–c30)
295 were identified, with nearly all samples contributing to each cluster (Figure 5B). Nine major cell
296 groups were identified (Figure 5C), based on their expression of marker genes (Figure 5D) (Niu
297 and Spradling, 2020; Morris et al., 2022). These comprised 10 granulosa cell clusters, 8 stromal
298 cell clusters, as well as theca cells, hematopoietic cells, endothelial cells, pericytes, smooth
299 muscle cells, and epithelial cells. Four clusters with low UMIs (c6, c11, c15, and c29) were
300 excluded from subsequent analysis (Figure S5A). Additionally, cluster c14 was removed due to
301 potential doublets, as it overlapped with several other clusters; however, we cautiously named it
302 'to be determined' (Figure S5B). Notably, all known ovarian somatic cell types were identified
303 within one or more clusters, but germ cells probably were too rare in these juvenile ovaries to
304 form a cluster, although ovarian germ cells have been extensively studied at earlier times by
305 these methods (Niu and Spradling, 2022) or similar stages using different methods (Morris et al.,
306 2022; Isola et al., 2024).

307 The initial clustering further validated the picture of wave 1 development obtained from
308 lineage studies. Cluster c1 expressed wave 1 BPG granulosa cell markers like *Nr5a2*, *Hsd3b1*,
309 and *Inha*, *Inhba* and increased 4-fold in cell number between wk2-wk4, before falling at wk 5 as
310 wave 1 granulosa cells turn over (Supplemental Dataset S6). Cluster c16 highly expressed theca
311 cell steroidogenic genes such as *Cyp11a1*, *Cy17a1*, and *Plin1*. The number of c16 cells peaked at
312 puberty (wk5). The outer "theca externa" is enriched in angiogenic cells, blood vessels, and
313 fibroblastic cells. Clusters corresponding to endothelial cells expressing *Flt1* (c22) and blood
314 cells expressing *Laptm5* (c23), increased nearly 4-fold between wk3 and wk5, consistent with
315 such vascularization.

316 **Analyzing GC gene expression**

317 We re-clustered the 10 initial GC clusters in Seurat, yielding 18 new clusters gc0-gc17
318 (Figure 6A) and classified them into groups corresponding to their likely association with
319 primordial (gc11), primary (gc3, gc8), secondary (gc1, gc4, gc9), antral (gc2, gc7, gc10, gc13),
320 and remodeling (gc0, gc6) follicles, as well as mitotically cycling cells(gc5, gc12, gc14, gc15,
321 gc16, and gc17) (Figure 6B, C). GCs from all follicle stages were identified across all samples
322 (Figure S5C). Single cell pseudotime trajectory analysis using Monocle3 identified distinct
323 developmental paths from primordial follicles to either antral follicles or remodeled follicles
324 (Figure 6D). Once primordial follicles reached the secondary stage, some progressed along path
325 1 toward antral follicles, while others followed path 2 toward remodeled follicles.

326 We identified up to 250 top differentially expressed genes for each group (Supplemental
327 Dataset 5) and carried out further analysis (Metascape: Zhou et al. 2019). The development and
328 remodeling of wave 1 follicles, and of boundary follicles giving rise to early wave 2 follicles is
329 summarized in Figure 7.

330 **Comparing gene expression in wave 1 vs wave 2 follicle development**

331 Wave 1 and wave 2 follicles begin to differ in gene expression early in fetal development,
332 as BPGs and EPGs express different genes as early as E14.5 and diverge further by P5 (Niu and
333 Spradling, 2020). To investigate whether gene expression differences at follicle formation persist
334 and to look for additional wave-specific gene expression, we examined GC clusters gc2, gc7,
335 gc10 and gc13 at 2wk, comprising all GC clusters scored as in antral follicles (Figure 5A, C). As
336 illustrated in Figure 7, only wave 1 antral follicles are present in significant numbers at wk2 and
337 wk3, prior to widespread wave 1 remodeling. In contrast, because of extensive wave 1 granulosa
338 cell turnover, by wk 5 nearly all these same antral follicle clusters come from developing

339 boundary follicles. Consequently, we compared gene expression levels during these two-time
340 intervals for all four antral granulosa cell clusters.

341 The nuclear receptor *Nr5a2*, is preferentially expressed 7.8-fold higher at P5 in BPGs
342 within growing wave 1 follicles compared to EPGs in growth-arrested wave 2 follicles (Niu and
343 Spradling, 2020). Similarly, *Nr5a2* expression is 11-fold higher in all wk2 antral follicle cell
344 clusters compared to primordial follicle (gc11) granulosa cells. This difference reflects the early
345 activation of wave 1, as *Nr5a2* turns on in all wave 2 GCs as they begin to grow (Meinsohn et al.
346 2019). We observed that *Nr5a2* expression increases in primary and secondary follicles and
347 reaches similar levels in wave 1 and wave 2 antral follicles (ratio = 1.02+/- 0.23). Comparable
348 expression ratios were likewise seen between wave 1 and wave 2 antral granulosa cells for other
349 genes that were BPG/wave 1-preferential at P5, including *Dhh* (1.04+/- 0.41), *Hsd17b1* (0.61+/-
350 0.14), *Ptgis* (1.08+/- 0.26), *Prlr* (1.8+/- 0.80), *Fshr* (0.89+/- 0.21) and *Igf1* (0.86+/- 0.10).

351 However, some genes continued to be differentially expressed between wave 1 and wave
352 2 follicles at the same stage of development. Wave 1 wk2 antral GCs express *Wnt4* at much
353 higher levels (4.8 +/- 1.0) compared to Wave 2 antral CGs at either wk 5 (0.17 +/- 0.069) or wk 6
354 (0.14 +/- 0.070). Other genes expressed more highly in wave 1 than wave 2 antral GCs are
355 *Igfbp5* (ratio: 27 +/- 10); *Itga6* (ratio: 6.28 +/- 0.97) and *Inha* (ratio: 1.52 +/- 0.29). Genes
356 expressed at lower levels in wave 1 than wave 2 include: *Cald1* (ratio: 0.20 +/- 0.089), *Ghr*
357 (ratio: 0.16 +/- 0.027), *Grb14* (ratio: 0.23 +/- 0.092), and *Mmp11* (ratio: 0.46 +/- 0.23). Thus,
358 gene expression is not entirely equivalent in wave 1 and wave 2 follicles at corresponding stages,
359 as has often been assumed.

360 Clusters gc0 and gc6 showed indications they derived from remodeling wave 1 follicle.
361 For example, the number of gc0 and gc6 cells is low at 2 and 3 wk before substantial atresia, but

362 jumps 9.8-fold at wk 4 (Supplemental Dataset 6). Preferentially expressed genes in gc0 and gc6
363 include *Cyp1b1*, *Atf3*, *Cxcl1*, *Bmp2*, *Apoe* and *Sox4*. Metascape analysis identified vasculature
364 development (-7.7; -4.0) cell cycle (-6.7; -9.2), and positive regulation of programmed cell death
365 (-4.1; nd), where the numbers indicate (q values log10 for gc0; gc6). These findings suggest
366 genes and pathways that GCs on remodeling wave 1 follicles use to stimulate vasculature
367 development, and ultimately to promote GC population turnover during wk4.

368 **Analyzing mesenchymal and steroidogenic gene expression**

369 We also re-clustered the mesenchymal cells, including theca cells and stromal cells,
370 yielding 21 new clusters to pursue a higher resolution picture of theca expansion (Figure 6E).
371 The re-clustered mesenchymal cells fell into nine groups, late-expanding TCs (g9), early TCs (g2
372 and g11), *Tagln*-expressing fibroblasts (g1, g8, g14 and g17), *Col14a1*-expressing fibroblasts
373 (g10 and g19), *Cd24a*-expressing fibroblasts (g4), *Cxcl12*-expressing fibroblasts (g3, g5 and
374 g20), *Hoxd9*-expressing fibroblasts (g0), *Col11a1*-expressing fibroblasts (g6 and g7) and mitotic
375 cells expressing *Mki67* (g12, g13, g15 and g18) (Figure 6F, S5D). The expression of genes in
376 cluster16 is hard to be determined still and be named in TBD. Theca cells in g9 highly expressed
377 steroidogenic genes such as *Star*, *Cyp11a1*, *Hsd3b1*, and *Cyp17a1* throughout wk2-wk6 and
378 peaked in expression and cell number at w5. In contrast, TCs in cluster g11 exhibited relatively
379 low levels of steroidogenic enzymes and stable cell numbers except at wk 5 where levels greatly
380 increased to reach 20-50% of g9 levels. Both groups expressed LH receptor (*Lhcgr*) and
381 prostaglandin E synthase 2 (*Ptges2*), previously implicated in TC androgen production (Erikson
382 et al. 1985), but Lhcgr levels in g11 started lower and increased more dramatically at wk 5 than
383 in g9.

384 Theca cells are not genetically capable of converting their androgen products into
385 estrogen and usually rely on exporting them to granulosa cells for this purpose (Edstrom et al.
386 2007). *Star*, a crucial gene responsible for transporting cholesterol from the cytoplasm into
387 mitochondria, is essential for steroidogenesis. The percentage of STCs expressing *Star* increased
388 from approximately 50% to over 80% at wk 5 (Figure 6G). Our findings demonstrate that STCs
389 increase in number and acquire a full complement of androgen biosynthetic enzymes during peri-
390 puberty. In contrast, GCs expressing *Hsd3b1*, *Cyp19a1*, and *Hsd17a1* indicating the potential to
391 synthesize estrogen peaked at wk 6 (Figure 6H), consistent with estrogen levels lagging
392 androgen levels during puberty (Galas et al. 2012; Trova et al. 2021).

393

394 DISCUSSION

395 **Wave 1 follicular remodeling generates a cluster of androgen-producing cells in the juvenile**
396 **mouse ovary**

397 Our work characterizes in detail the development of the first wave of mouse ovarian
398 follicles at the cellular and gene expression levels. In agreement with earlier studies (Hirshfield
399 and DeSanti, 1995; Gougeon, 1996; McGee and Hsueh, 2000; Eppig and Handel, 2012), 80-
400 100% of these follicles turn over rather than generating fertilizable oocytes. We document the
401 cellular and genetic changes within each major follicular cell type and detail the complex events
402 that ultimately produce a large cluster of amplified steroidogenic theca cells and interstitial gland
403 cells along with a residue of granulosa cells within the ovarian medulla by 5 wk. This process
404 was previously termed wave 1 follicle atresia and was known to be associated with increased
405 steroidogenesis and vascularization (Magoffin, 2005). Our analysis characterizes the cellular and
406 molecular programs in each wave 1 follicular cell type that cause them to turn over, remodel,

407 change in number, associate with new mesenchymal cells and to modulate their gene expression
408 to produce steroid hormones from the ovary in a timely fashion during juvenile development.
409 Our findings show that wave 1 follicles play a role in steroid production during juvenile
410 development, especially at the puberty.

411 **Wave 1 follicles give rise to few mature oocytes that generate offspring**

412 Boundary follicles as well as wave 1 follicles were labeled in our *Foxl2* lineage tracing
413 experiments, and in early experiments of Zheng et al. 2014a. Boundary primordial follicles
414 activate as early as 2 wk and produce most of the first follicles to develop fully, ovulate and
415 generate offspring (Figure 3). It remains possible that a small number of wave 1 follicles, ~26 or
416 fewer, do develop to maturity. However, their contribution of wave 1 to fertility is minor at most.
417 Thus, early activated wave 2 follicles at the medulla-cortex boundary rather than wave 1 follicles
418 are largely responsible for early fertility. Most non-boundary wave 2 follicles only begin to
419 activate between puberty and sexual maturity, possibly in concert with the onset of pulsatile
420 hypothalamic-pituitary-gonadal axis activity.

421 **Wave 1 follicles may be a conserved feature in other animals including humans**

422 The developing ovaries of many species produce follicles that do not complete oogenesis
423 and ovulate (Jiménez, 2009; DeFalco and Capel, 2009). For example, an early wave of germ
424 cells in *C. elegans* hermaphrodites develop into sperm, while during adult life only oocytes are
425 generated (Pazdernik and Schedl, 2013). An initial wave of germ cells in the mouse testis
426 develop during juvenile stages but break back down into individual cells, possibly to expand the
427 stem cell pool (Lei and Spradling, 2013). Primordial germ cells in Drosophila pupal ovaries
428 develop directly into the first ovulated oocytes, while all subsequent oocytes derive from
429 germline stem cells that provide lifelong fertility (Zhu and Xie, 2003).

430 Human follicles begin developing, as in mouse, long before there is any prospect of
431 ovulation. A fraction of primordial human follicles start to form during fetal stages, and 4-6%
432 have progressed to the primary follicle stage prior to birth (Forabosco and Sforza, 2007). Such
433 early developing follicles have no prospect of surviving 8 to 13 more years until the onset of
434 puberty when they might contribute to fertility. Juvenile human ovaries 3 mo to 8 yr in age also
435 contained 2-13% of small growing follicles that had diverged from a normal developmental
436 pattern. 50-60% of large follicles showed signs of atresia including loss of oocytes and most
437 granulosa cells, but retention of some theca cells (Himelstein-Braw et al., 1976). Currently, there
438 is little understanding of the developmental mechanisms or logic underlying human fetal and
439 juvenile follicle production. Early follicles in humans might undergo atresia and remodeling to
440 enhance production of androgens or other steroid hormones to influence organ and brain
441 development (Cui et al., 2013; Bell, 2018). These studies on the development of mouse wave 1
442 follicles and their component cell types should aid in understanding early follicular waves in
443 many species.

444 **Identification of the earliest activating wave 2 follicles at the medullary-cortex boundary**

445 A long-standing question in mammalian reproduction has been the activation order of
446 quiescent wave 2 primordial follicles during the life cycle (McGee and Hsueh, 2000). In
447 addition to over 250 wave 1 follicles in the medulla that begin rapid growth at birth, we
448 identified more than 400 wave 2 primordial follicles near the medullar-cortical boundary whose
449 GCs in 2 wk ovaries are also labeled in a mosaic fashion with *Foxl2-CreERT2* is activated at
450 E16.5 or even earlier. Boundary follicles appear to correspond largely or entirely the primordial
451 follicle subclass poised for early activation and located at the medulla-cortical boundary
452 (Meinsohn et al. 2021a, b). Our data show that his substantial class of early primordial follicles

453 do begin developing shortly after 2 wk, giving them sufficient time to become secondary and
454 antral follicles at 5 wk. It remains possible that a small number of wave 1 follicles, ~26 or fewer,
455 do develop to maturity. However, it seems clear that the great majority of early progeny derive
456 from boundary or other early developing wave 2 follicles, rather than wave 1 follicles that escape
457 atresia.

458 **Mouse follicle waves express distinct genes**

459 We found that differences in gene expression between wave 1 and wave 2 granulosa cells
460 exist and may contribute or even control the different fates of mouse follicular waves.
461 Previously, gene expression differences had been mapped beginning as early E14.5, and many
462 were characterized between E16.5 to P5 (Niu and Spradling, 2020). They suggested that wave 1
463 follicles in the medulla differentially express several genes involved in steroid hormone
464 production, while wave 2 granulosa cells in the cortex express genes that might predispose
465 follicles to enter quiescence. This study extends knowledge of differences in gene expression
466 within follicular waves during juvenile development up to 6 wk. Wave 1 follicles express much
467 higher levels of *Wnt4* and *Igfbp5* than wave 2 follicles. Wnt4 has been genetically linked in
468 humans to Mullerian dysgenesis and hyperandrogenism (Choussein et al. 2017) perhaps
469 reflecting its known roles in promoting female vs male development. High *Wnt4* expression in
470 wave 1 granulosa cells may indicate that *Wnt4*-mediated downregulation of androgen production
471 at 2 wk becomes reduced by granulosa cell degradation, promoting the subsequent upregulation
472 of androgen levels at puberty. *Igfbp5*, the most highly conserved of the Igfbp's, is also a potent
473 regulator of female reproductive tissue (Schneider et al. 2002). Thus, while changing levels of
474 gonadotrophins in young juvenile mice likely play a role in wave 1 atresia (Edson et al., 2009),

475 intrinsic differences in gene expression within different follicular waves at the same stage exist
476 and have the potential to be important.

477 **The timing of follicular activation begins to be specified early in ovarian development**

478 Finding that a subset of primordial follicles located near the medulla-cortex border
479 comprise many of the earliest activated wave 2 follicles raised the question how early activation
480 is controlled. It is well established that upregulation of insulin-mediated growth pathways
481 accompanies follicle activation (Edson et al., 2009). Boundary follicles may become poised to
482 active before most other wave 2 follicles because their location close to the nutrient-rich medulla
483 enhances growth signaling, weakens quiescence and activates *Nr5a2* and *Foxl2* expression,
484 genes which are expressed in GCs of all growing follicles. Wave 1 granulosa cells in the
485 medulla differentially express genes promoting growth like *Igfbp5*, *Grb14* and *Ghr*, and
486 signaling genes like *Itga6* and *Inha*, relative to wave 2 follicles growing during wks 4 and 5.

487 However, evidence increasingly suggests that follicular waves do not simply depend on
488 differences in their local microenvironments. These follicle groups form at times in fetal ovary
489 development that overlap other critical events of gonad development. The progenitors of
490 bipotential reproductive cell types like BPGs and and mesenchymal steroidogenic precursors that
491 arise early in both male and female gonad development remain elusive (Meinsohn, 2005; Edson
492 et al. 2009). These cells include stem-like cells that give rise to theca cells and interstitial gland
493 cells. We were able to preferentially mark both wave 1 follicles and boundary follicles using
494 *Foxl2-CreERT2* as early as E14.5, suggesting that they are specified as early as bipotential and
495 later progenitors, and involve intercellular signaling events linked to sex determination. Progress
496 in understanding basic questions of gonad development would undoubtedly advance insight into
497 how wave 1 and boundary follicles are specified.

498 **Genetic studies of wave 1 follicles**

499 We explored genotypes that reduce the number of wave 1 follicles in order to look for the
500 genetic consequences of decreased wave 1 activity. In Turner syndrome, wave 1 follicle
501 development is reported to be reduced significantly (Miura et al. 2017). This imbalance might
502 decrease androgen levels, potentially affecting juvenile development. Consistent with hormonal
503 disruption, hormone replacement therapy significantly improves the development of individuals
504 with Turner syndrome (Klein et al., 2018). Moreover, androgens are known to play an important
505 role in this effect (Zuckerman-Levin et al., 2009; Viuff et al., 2022).

506 We examined mouse XO mice and looked for changes in wave 1 follicle numbers (Figure
507 S7B-C). In our experiments, wave 1 follicle numbers were reduced relative to levels in XX
508 control females at wk1 of development. However, the reduction was transient and by 2 wk,
509 before remodeling and theca cell expansion, XO and XX females had regained a similar number
510 of wave 1 follicles. Consequently, we could not draw any conclusions regarding the functional
511 role of wave 1 follicles and their remodeling from these studies.

512 **Steroid hormones mediate sexual development in juvenile mice and during peri-puberty**

513 Steroid hormones influence the development of sexually dimorphic organs including the
514 brain (review Simerly, 2002; Arnold, 2009). They have multiple sources, including steroids in the
515 maternal circulation during pregnancy, as well as subsequent systemic and local steroid
516 production during juvenile stages. Wave 1-derived theca cell numbers are high during wk 4-5 of
517 juvenile development. a period known as peri-puberty that has been associated with sexual
518 behavior development and with high levels of androgens, as well as relatively low estrogen
519 production (François et al. 2017; Trova et al. 2021; Devillers et al., 2023). While the sensitivity

520 of the brain to steroid influences is probably declining during this period, sexually dimorphic
521 circuits are still being shaped in a manner that is important for sexually dimorphic behaviors in
522 female and male rodents (Sisk and Zehr, 2005; Templin et al., 2019; Trova et al., 2021; Yoest et
523 al., 2023). Potential targets of this influence include the anteroventral periventricular nucleus
524 (AVPV) which is larger in female than male rodents and helps regulate female reproductive
525 functions such as ovulation and gonadotrophin production. Sex hormones produced in females
526 during puberty also enhance cell death in the primary visual cortex, reducing its volume in
527 females compared to males. Thus, wave 1 generated steroid production may influence the sexual
528 development.

529 **Wave 1 follicle remodeling, polycystic ovarian syndrome and human follicular waves**

530 The work reported here may be relevant to the origin and high frequency of polycystic
531 ovary syndrome (PCOS) (McCartney and Marshall, 2016). A possible connection between
532 follicular atresia, androgen excess and PCOS has been discussed previously (reviewed in Erikson
533 et al., 1985; Magoffin, 2005). Interestingly, some histological characteristics of remodeling
534 mouse wave 1 follicles resemble follicles within the ovaries of individuals with PCOS (Chang,
535 2007; Franks and Hardy, 2010; Walters et al., 2019). A good place to start toward further
536 progress on this connection would be to characterize the development and gene expression of
537 early human follicles and compare them to the findings reported in other systems, including
538 mice.

539

540 # MATERIALS AND METHODS

541 **Antibodies**

542

Name	Source	Identifier	Dilution
Anti-EGFP (Chicken)	Aves labs	GFP-1020	1:300
Anti-DDX4 (Rabbit)	Abcam	ab13840	1:300
Anti-MSY2 (Mouse)	Abcam	sc-393840	1:100
Anti-tdTomato (Goat)	Origene Tech	AB8181-200	1:300
Anti-HSD3B1 (Mouse)	Santa Cruz	sc-515120	1:100
Anti-CYP17A1 (Rabbit)	Cell Signaling Technology	94004T	1:100
Anti-PLIN1 (Rabbit)	abcam	ab3526	1:100
DAPI	Sigma	D9542-10mg	0.5ug/ml
Alexa Fluor® 488 AffiniPure™ Donkey Anti-Chicken IgY (IgG) (H+L)	Jacksonimmuno	703-545-155	1:300
Alexa Fluor® 594 AffiniPure™ Donkey Anti-Goat IgG (H+L)	Jacksonimmuno	705-585-147	1:300
Alexa Fluor 488 donkey anti-mouse lgG	invitrogen	A21202	1:300
Alexa Fluor 568 donkey anti-mouse lgG	invitrogen	A10037	1:300
Alexa Fluor 488 donkey anti-rabbit lgG	invitrogen	A21206	1:300
Alexa Fluor 568 donkey anti-rabbit lgG	invitrogen	A10042	1:300
Alexa Fluor 647 donkey anti-rabbit lgG	invitrogen	A31573	1:300

543 **Primers**

Name	Forward (5'-3')	Reverse (5'-3')	Size	Chromosome	Note
XO-qPCR-Tg	GACTAGGTTCATAGGCACTGG	CCGCCAAAACTCCTTCTCTAC	123 bp	X	Genotyping for XO mice
XO-qPCR-Tg-Probe	[5HEX]CCCCAGATGGTACCCACAGAACTTG			X	
XO-qPCR-IPC	CACGTGGGCTCCAGCATT	TCACCAGTCATTTCTGCCTTTG	74 bp	12	
XO-qPCR-IPC-Probe	[Cy5]CCAATGGTCGGGCACTGCTCAA			12	
Foxl2-Mutant	AGAGAAGAGAGTGAGAGCCG	GTCCAGCTCGACCAGGATGG	221 bp	9	Genotyping for Foxl2-CreERT2
Foxl2-WT	AGAGAAGAGAGTGAGAGCCG	GAGCGCCACGTACGAGTACG	335 bp	9	
Cyp17a1-Tg	GCTGTAGCTTCTCCACTCCAC	CAGGTTTTGGTGCACAGTCA	120 bp		Genotyping for Cyp17a1-iCre
Cyp17a1-IPC	AGTGGCCTCTTCCAGAAATG	TGCGACTGTGTCTGATTTCC	521 bp		

544

545

546 **Experimental mice**

547 All animal experiments were conducted in compliance with the Institutional Animal Care
548 and Use Committee guidelines of the Carnegie Institution of Washington (CIW). The mice were
549 housed in specific pathogen-free facilities at CIW. The strains of mice used in the study were
550 acquired from Jackson Laboratory, including C57BL/6J (B6, strain #: 000664), DBA/2J (DBA2,
551 strain #: 000671), B6;129P2-*Foxl2*$^{tm1(GFP/cre/ERT2)Pzg}$/J (*Foxl2-CreERT2*, strain #: 015854),
552 STOCK XO/J (XO, strain #: 036414), B6CBACaF1/J-*A*$^{w-J}$/*A* (Strain #:001201) and B6;SJL-
553 Tg(Cyp17a1-icre)AJako/J (*Cyp17a1-icre*, strain #: 028547). The *R26R-LSL-EYFP* reporter mice
554 B6.129X1-*Gt(ROSA)26Sor*$^{tm1(EYFP)Cos}$/J (*R26R-LSL-EYFP*, strain #: 006148) were acquired from
555 Jackson Laboratory and backcrossed onto 129S1/SvImJ (129S1, strain #: 002448) background in
556 our lab. The R26R-LSL-tdTomato reporter mice were generously provided by Chen-Ming Fan at
557 the CIW. CD-1 IGS Mouse (strain #: 022) was obtained from Charles River Laboratories.

558 **Lineage tracing experiments**

559 To visualize the expression patterns of *Foxl2* and *Cyp17a1*, we generated reporter mouse
560 lines by crossing *R26R-EYFP* or *R26R-tdTomato* mice with *Foxl2-CreERT2* or *Cyp17a1-iCre*
561 (Shimshek et al., 2002; Zhou et al., 2022) mice. The presence of a vaginal plug was designated
562 as embryonic day 0.5 (E0.5). Pregnant females were injected intraperitoneally (IP) with 1 mg
563 tamoxifen (TAM) (MilliporeSigma, #T5648, 10 mg/ml dissolved in corn oil) per 35 g body
564 weight at E16.5 or E14.5 (*Foxl2-CreERT2*). Pups were either delivered naturally or, if not born
565 on the expected delivery day, delivered by C-section and fostered by a CD1 female mouse. The
566 day of birth was considered postnatal day 0 (P0). We collected gonads from fetuses or ovaries
567 from pups at the indicated stages for analysis. All experiments were conducted with at least three

568 biological replicates from two litters and were repeated twice. The loss of one *Foxl2* allele in
569 *Foxl2-CreERT2* mice, along with tamoxifen administration, does not significantly impact
570 ovarian development or overall mouse health.

571 To investigate the expression of *Foxl2* in remodeled follicles, tamoxifen was injected IP
572 at a concentration of 1 mg per 35 g weight into female mice at 5 weeks of age. The ovaries were
573 dissected one week later and subjected to whole mount staining for analysis.

574 **Immunostaining**

575 Whole-mount staining was performed as previously described (Li et al., 2017). Briefly,
576 gonads or ovaries were fixed in 4% paraformaldehyde (PFA) overnight at 4°C. The tissues were
577 then washed three times in a washing buffer (0.3% Triton X-100 and 0.5% thioglycerol in PBS)
578 and incubated in blocking buffer (1% normal donkey serum, 1% BSA, and 0.3% Triton X-100 in
579 PBS) overnight at 37°C. The samples were incubated with primary antibody in dilution buffer
580 (1% BSA and 0.3% Triton X-100 in PBS) for two days at 37°C. After washing in the washing
581 buffer overnight at 37°C, the samples were incubated with secondary antibodies in dilution
582 buffer for another two days at 37°C, followed by washing in the washing buffer with DAPI
583 overnight at 37°C. To facilitate whole-tissue imaging, the clearing buffer Ce3D (prepared by
584 dissolving 4 g Histodenz in 2.75 ml of 40% [v/v] N-methylacetamide) was applied for an
585 additional day. The samples were imaged using a Leica TCS SP8 confocal microscope or a Leica
586 Stellaris 8 DIVE confocal microscope. Images were analyzed using Fiji or Imaris.

587 For fluorescence cryosection staining, the dissected tissues were fixed in 4% PFA
588 overnight at 4°C. After washing three times in PBS, the tissues were dehydrated sequentially in
589 10% and 30% sucrose solutions and embedded in O.C.T. for cryosectioning. The slides were

590 sectioned at a thickness of 5 μm and stored at -20°C until staining. After antigen retrieval in
591 0.01% sodium citrate buffer at boiling temperature for 20 minutes, the slides were sequentially
592 blocked for 1 hour at room temperature, incubated with primary antibodies overnight at 4°C, and
593 then with secondary antibodies for 1 hour at room temperature. This was followed by
594 counterstaining with DAPI for 10 minutes before fixing in mounting medium. The samples were
595 then imaged with an upright SP5 microscope, and the images were analyzed using Fiji.

596 **Oil Red O Staining**

597 Oil Red O Staining was performed using Oil Red O stain kit (Abcam, ab150678)
598 following the manufacturer's protocol. Briefly, the slides were placed in propylene glycol for 5
599 minutes at room temperature, followed by incubation in Oil Red O solution at 60°C for 10
600 minutes. The slides were then differentiated in 85% propylene glycol for 1 minute, followed by
601 rinsing twice in distilled water. The slides were then incubated in hematoxylin for 1 minute,
602 rinsed thoroughly in tap water and twice in distilled water. The slides were ready for imaging
603 after applying a coverslip using an aqueous mounting medium. Imaging was done using a Nikon
604 Eclipse E800 microscope.

605 **Genotyping**

606 The tissue was dissected and incubated in a lysis buffer (30 mM Tris-HCl, 0.5% Triton
607 X-100, 200 μg/ml Proteinase K) at 55°C overnight in a water bath. The lysis buffer was then
608 inactivated by heating at 95°C for 5 minutes.

609 For genotyping using conventional PCR, 1 μl of the sample was added to the PCR
610 mixture (primer sequences are provided in the supplemental data). For quantitative PCR (qPCR)
611 to genotype XO mice, primers and probes (sequences included in the supplemental data) were

612 designed to amplify and detect target DNA sequences from both the X chromosome and an
613 autosome. qPCR was performed using a CFX 96 Real-Time PCR machine. The amplification
614 cycle threshold for the X chromosome was compared to that of the autosome to determine the
615 genotype, distinguishing between XO (one X chromosome) and XX (two X chromosomes)
616 females.

617 **Single cell RNA sequencing**

618 Tissue samples were first dissected in PBS and dissociated using 0.25% Trypsin/EDTA
619 (Thermo Fisher, #25200056) at 37°C for approximately 20 minutes. Dissociation was halted by
620 adding FBS (Thermo Fisher, #10439016) to a final concentration of 10%. The resulting cell
621 suspension was filtered through a 100 µm strainer (Fisher, #22-363-549) to remove any
622 remaining undissociated structures. Cells were pelleted by centrifugation using an Allegra X-14R
623 Centrifuge (Beckman Coulter) at 300 × g for 3 minutes and suspended in PBS containing 0.04%
624 BSA (PBSB). To further eliminate cell clumps, the samples were filtered through a 40 µm
625 strainer (Fisher, #22-363-547), followed by centrifugation at 300 × g for 5 minutes. The cells
626 were then resuspended in PBSB and subjected to FACS sorting (BD FACSAria™ III Cell Sorter)
627 to collect live cells, with SYTOX™ Orange Dead Cell Stain (Thermo Fisher, S34861) used for
628 viability selection. After a final centrifugation at 300 × g for 5 minutes, the cells were
629 resuspended in appropriate volume of PBSB to achieve a concentration of 1000 cells/µl before
630 proceeding with single-cell sequencing.

631 Libraries of the single cells were prepared using the Chromium Next GEM Single Cell 3'
632 Reagent Kits v3.1(PN-1000128) from 10X Genomics, with the goal of capturing 10,000 cells per
633 sample. Sequencing was performed using the NextSeq 500 platform from Illumina according to
634 10X Genomics recommendations: paired-end, single index reads with Read 1 being 28 cycles,

635 Index 1 being 8 cycles, and Read 2 being 91 cycles. Sequencing was performed to a depth of
636 50,000 reads per cell. The single cell sequencing datasets were initially processed using the Cell
637 Ranger pipeline (v3.1.0 and v6.0.1) with default settings.

638 Further analysis of the scRNA-seq data was performed using the Seurat package (v4.1.0).
639 The count data were read and transformed into a Seurat object using the 'Read10X' and
640 'CreateSeuratObject' functions. The libraries (2 weeks, 3 weeks, 4 weeks, 5 weeks, and 6 weeks)
641 were preprocessed with 'NormalizeData()', followed by 'FindVariableFeatures()',
642 'FindIntegrationAnchors()', and 'IntegrateData()' using default settings. The integrated object
643 was further processed using 'ScaleData()', 'RunPCA(npcs = 50)', 'RunUMAP(dims = 1:30)',
644 'FindNeighbors(dims = 1:30)', 'FindClusters(resolution = 1.0)', and 'RunTSNE(dims = 1:30)'
645 with other default settings to determine cell clusters. Further clustering of granulosa cells and
646 mesenchymal cells was performed using 'subset ()', followed by the cell clustering methods
647 mentioned above.

648 **The electron microscope**

649 Mice ovaries were excised and fixed in a solution of 2% PFA and 2.5% glutaraldehyde in
650 0.1 M PIPES buffer (MilliporeSigma, #P6757, pH 7.4) at 4°C overnight. The ovaries were then
651 washed and treated with 50 mM glycine in 0.1 M PIPES buffer for 15 minutes, followed by
652 washing with 0.1 M PIPES buffer. Tissue pieces were then postfixed with 1% osmium tetroxide
653 and 1.5% potassium ferrocyanide in 0.1 M PIPES buffer for 60 minutes, washed with water, and
654 stained en bloc with 1% (w/v) uranyl acetate for 60 minutes. The ovaries were then serially
655 dehydrated using graded ethanol solutions: 30%, 50%, 75%, 85%, 95%, and 100% ethanol,
656 followed by two exchanges of 100% acetone. After dehydration, the ovaries were infiltrated and
657 embedded in EMbed 812 Epoxy resin (Electron Microscopy Sciences) according to the

658 manufacturer's recommendations. Ultrathin sections at about 70 nm thick were cut on a Leica
659 EM UC7 ultramicrotome and examined using a Hitachi HT7800 transmission electron
660 microscope operated at 80 kV. Images were acquired with an AMT NanoSprint 12 camera.

661 **Statistical analysis**

662 The data are reported as means ± SD of biological replicates, and no statistical methods
663 were used to determine the sample size. Differences between two groups were compared using a
664 two-tailed Student's *t*-test. A *p*-value of <0.05 was considered statistically significant and marked
665 with one star (*), $p < 0.01$ with two stars (**), $p < 0.001$ with three stars (***), and $p < 0.0001$
666 with four stars (****).

667 **Data availability**

668 The scRNAseq data have been deposited at the NIH GEO database under accession
669 number GSE268466.

670 **Funding**: Howard Hughes Medical Institute

671 **Supplementary Materials:**

672 Figs. S1 to S7

673 Movies S1 to S10

674 Datasets S1-S6

675 **ACKNOWLEDGEMENTS:** We are grateful to Allison Pinder and Dr. Fredrick Tan for
676 assisting with the genomic experiments and analyses. We thank Dr. Mamhud Siddiqi for his help
677 with optical microscopy and image analyses. We thank Dr. Ru-Ching Hsia for expert electron
678 microscopy. We thank the Carnegie Embryology support staff and Spradling lab members for
679 comments on the study, especially Haolong Zhu for assistance with scRNA-seq data analysis.

680 **Author contributions:** Investigation: QY, Supervision and Funding: ACS, all other: QY and
681 ACS.

682 **Competing interests:** None.

683

684 # REFERENCES

685 Arnold AP. (2009). The organizational-activational hypothesis as the foundation for a unified
686 theory of sexual differentiation of all mammalian tissues. Horm Behav. 5, 570-8. doi:
687 10.1016/j.yhbeh.2009.03.011.

688 Bell MR (2018). Comparing Postnatal Development of Gonadal Hormones and Associated
689 Social Behaviors in Rats, Mice, and Humans. Endocrinology 159, 2596-2613. doi:
690 10.1210/en.2018-00220.

691 Bianco S, Bellefleur AM, Beaulieu É, Beauparlant CJ, Bertolin K, Droit A, Schoonjans K,
692 Murphy BD & Gévry N (2019). The ovulatory signal precipitates LRH-1 transcriptional
693 switching mediated by differential chromatin accessibility. Cell Reports 27 2443.e4–2454.e4.
694 doi: 10.1016/j.celrep.2019.07.088.

695 Bridges PJ, Koo Y, Kang DW, Hudgins-Spivey S, Lan ZJ, Xu X, DeMayo F, Cooney A, Ko C.
696 (2008) Generation of Cyp17iCre transgenic mice and their application to conditionally delete
697 estrogen receptor alpha (Esr1) from the ovary and testis. Genesis 46(9):499-505. doi:
698 10.1002/dvg.20428.

699 Byskov, AG (1974). Cell kinetic studies of follicular atresia in the mouse ovary. J. Reprod. Fert.
700 37, 277-285. doi: 10.1530/jrf.0.0370277.

701 Chang RJ. (2007). The reproductive phenotype in polycystic ovary syndrome. Nat Clin Pract
702 Endocrinol Metab. 3, 688-95. doi: 10.1038/ncpendmet0637.

703 Chen YY, Russo DD, Drake RS, Duncan FE, Shalek AK, Goods BA, Woodruff TK. (2022).
704 Single-cell transcriptomics of staged oocytes and somatic cells reveal novel regulators of follicle
705 activation. Reproduction. 164(2):55-70. doi: 10.1530/REP-22-0053.

706 Choussein S, Nasioudis D, Schizas D, Economopoulos KP. (2017). Mullerian dysgenesis: a
707 critical review of the literature. Arch Gynecol Obstet. 295:1369-1381. doi: 10.1007/s00404-017-
708 4372-2.

709 Cui J, Shen Y, Li R. (2013). Estrogen synthesis and signaling pathways during aging: from
710 periphery to brain. Trends Mol Med. 19, 197-209. doi: 10.1016/j.molmed.2012.12.007.

711 DeFalco T, Capel B (2009). Gonad morphogenesis in vertebrates: divergent means to a
712 convergent end. Annu. Rev. Cell Dev. Biol. 25, 457-482. doi:
713 10.1146/annurev.cellbio.042308.13350

714 Devillers MM, François CM, Chester M, Corre R, Cluzet V, Giton F, Cohen-Tannoudji J, Guigon
715 CJ. (2023). Androgen receptor signaling regulates follicular growth and steroidogenesis in
716 interaction with gonadotropins in the ovary during mini-puberty in mice. Front Endocrinol
717 (Lausanne). 14, 1130681. doi: 10.3389/fendo.2023.1130681.

718 Duggavathi R, Volle DH, Mataki C, Antal MC, Messaddeq N, Auwerx J, Murphy BD &
719 Schoonjans K (2008). Liver receptor homolog 1 is essential for ovulation. Genes and
720 Development 22 1871–1876. doi: 10.1101/gad.472008.

721 Edson MA, Nagaraja AK, Matzuk MM. (2009). The mammalian ovary from genesis to
722 revelation. Endocr Rev. 30, 624-712. doi: 10.1210/er.2009-0012.

723 Eppig JJ, Handel MA. (2012). Origins of granulosa cells clarified and complexified by waves.
724 Biol Reprod 86, 34. doi: 10.1095/biolreprod.111.096651.

725 Erickson GF, Magoffin DA, Dyer CA, Hofeditz C. (1985). The ovarian androgen producing
726 cells: a review of structure/function relationships. Endocr Rev. 6, 371-99. doi: 10.1210/edrv-6-3-
727 371.

728 Faire M, Skillern A, Arora R, Nguyen DH, Wang J, Chamberlain C, German MS, Fung JC, Laird
729 DJ. (2015). Follicle dynamics and global organization in the intact mouse ovary. Dev Biol. 403,
730 69-79. doi: 10.1016/j.ydbio.2015.04.006.

731 Feng Y, Cui P, Lu X, Hsueh B, Möller Billig F, Zarnescu Yanez L, Tomer R, Boerboom D,
732 Carmeliet P, Deisseroth K, Hsueh AJ. (2017). CLARITY reveals dynamics of ovarian follicular
733 architecture and vasculature in three-dimensions. Sci Rep. 7, 44810. doi: 10.1038/srep44810.

734 Fiorentino G, Parrilli A, Garagna S, Zuccotti M. (2020). Three-Dimensional Micro-Computed
735 Tomography of the Adult Mouse Ovary. Front Cell Dev Biol. 8, 566152. doi:
736 10.3389/fcell.2020.566152.

737 Forabosco F, Sforza C. (2007). Establishment of ovarian reserve: a quantitative morphometric
738 study of the developing human ovary. Fertility and Sterility 88, 675-683. doi:
739 10.1016/j.fertnstert.2006.11.191.

740 François CM, Petit F, Giton F, Gougeon A, Ravel C, Magre S, Cohen-Tannoudji J, Guigon CJ.
741 (2017). A novel action of follicle-stimulating hormone in the ovary promotes estradiol
742 production without inducing excessive follicular growth before puberty. Sci Rep. 7, 46222. doi:
743 10.1038/srep46222.

744 Franks S, Hardy K (2010). Aberrant follicle development and anovulation in polycystic ovary
745 syndrome. Annales d'Endocrinologie 71, 228–230. doi: 10.1016/j.ando.2010.02.007

746 Galas J, Slomczynska M, Knapczyk-Stwora K, Durlej M, Starowicz A, Tabarowski Z, Rutka K,
747 Szoltys M. (2012). Steroid levels and the spatiotemporal expression of steroidogenic enzymes

and androgen receptor in developing ovaries of immature rats. Acta Histochem 114, 207–216. doi: 10.1016/j.acthis.2011.04.006.

Gougeon A. (1996). Regulation of ovarian follicular development in primates: facts and hypotheses. Endocr Rev 17:121–155. doi: 10.1210/edrv-17-2-121.

Guigon CJ, Mazaud S, Forest MG, Brailly-Tabard S, Coudouel N, Magre S. (2003). Unaltered development of the initial follicular waves and normal pubertal onset in female rats after neonatal deletion of the follicular reserve. Endocrinology. 144(8):3651-62. doi: 10.1210/en.2003-0072.

Guzmán A, Hughes CHK, Murphy BD (2022). Liver receptor homolog 1 (LHR-1) regulates follicle vasculature during ovulation in mice. Reproduction 164, 283-289. doi: 10.1530/REP-22-0135.

Guzmán A, Hernández-Coronado CG, Gutiérrez CG, Rosales-Torres AM. (2023). The vascular endothelial growth factor (VEGF) system as a key regulator of ovarian follicle angiogenesis and growth. Mol Reprod Dev. 90, 201-217. doi: 10.1002/mrd.23683.

Habara O, Logan CY, Kanai-Azuma M, Nusse R, Takase HM (2021). WNT signaling in pregranulosa cells is required for ovarian folliculogenesis and female fertility. Development. 148, dev198846. doi: 10.1242/dev.198846.

Himelstein-Braw R, Byskov AG, Peters H, Faber, M. (1976). Follicular atresia in the infant human ovary. Reproduction 46, 55-59. doi: 10.1530/jrf.0.0460055.

Hirshfield AN. (1992). Heterogeneity of cell populations that contribute to the formation of primordial follicles in rats. Biol Reprod 47:466–472. doi: 10.1095/biolreprod47.3.466.

Hirshfield AN, DeSanti AM. (1995). Patterns of ovarian cell proliferation in rats during the embryonic period and the first three weeks postpartum. Biol Reprod 1995;53:1208 –1221. doi: 10.1095/biolreprod53.5.1208.

Hogan, B, Beddington R, Costantini F, Lacy E. (1994). Manipulating the mouse embryo : a laboratory manual (2nd ed.). Cold Spring Harbor Laboratory Press.

Hsueh AJ, Billig H, Tsafriri A. (1994). Ovarian follicle atresia: a hormonally controlled apoptotic process. Endocr Rev. 15, 707-24. doi: 10.1210/edrv-15-6-707.

Isola JVV, Ocañas SR, Hubbart CR, Ko S, Mondal SA, Hense JD, Carter HNC, Schneider A, Kovats S, Alberola-Ila J, Freeman WM, Stout MB. (2024). A single-cell atlas of the aging mouse ovary. Nat Aging. 4(1):145-162. doi: 10.1038/s43587-023-00552-5.

Jiménez R. (2009). Ovarian organogenesis in mammals: mice cannot tell us everything. Sex Dev. 3, 2911-301. doi: 10.1159/000280584

Kelava I, Chiaradia I, Pellegrini L, Kalinka AT, Lancaster MA. (2022). Androgens increase excitatory neurogenic potential in human brain organoids. Nature 602, 112-116. doi: 10.1038/s41586-021-04330-4.

Klein KO, Rosenfield RL, Santen RJ, Gawlik AM, Backeljauw PF, Gravholt CH, Sas TCJ, Mauras N (2018). Estrogen Replacement in Turner Syndrome: Literature Review and Practical Considerations. J Clin Endocrinol Metab. 103, 1790-1803. doi: 10.1210/jc.2017-02183.

Lamas S, Carvalheira J, Gartner F, Amorim I. (2021). C57BL/6J mouse superovulation: schedule and age optimization to increase oocyte yield and reduce animal use. Zygote 29, 199-203. doi: 10.1017/S0967199420000714.

Lei L, Spradling AC. (2013). Mouse primordial germ cells produce cysts that partially fragment prior to meiosis. Development. 140(10):2075-81. doi: 10.1242/dev.093864.

Li W, Germain RN, Gerner MY. (2017). Multiplex, quantitative cellular analysis in large tissue volumes with clearing-enhanced 3D microscopy (Ce3D). Proc Natl Acad Sci U S A. 114, E7321-E7330. doi: 10.1073/pnas.1708981114.

Liu, C, Peng, J, Matzuk, MM, & Yao, HHC. (2015). Lineage specification of ovarian theca cells requires multicellular interactions via oocyte and granulosa cells. Nature commun, 6, 6934. doi: 10.1038/ncomms7934

Liu C, Rodriguez K, Yao HHC. (2016). Mapping lineage progression of somatic progenitor cells in the mouse fetal testis. Development. 143(20): 3700–3710. doi: 10.1242/dev.135756.

Magoffin DA. (2005). Ovarian theca cell. Int J Biochem Cell Biol. 37(7):1344-9. doi: 10.1016/j.biocel.2005.01.016.

Mawaribuchi S, Ikeda N, Fujitani K, Ito Y, Onuma Y, Komiya T, Takamatsu N, Ito M (2014). Cell-mass structures expressing the aromatase gene Cyp19a1 lead to ovarian cavities in Xenopus laevis. Endocrinology. 155(10):3996-4005. doi: 10.1210/en.2014-1096. Epub 2014 Jul 22.

McCartney CR. & Marshall JC. (2016). Polycystic ovary syndrome. N. Engl. J. Med. 375, 54–64. doi: 10.1056/NEJMcp1514916

McGee EA, Hsueh AJ. (2000). Initial and cyclic recruitment of ovarian follicles. Endocr Rev 21:200–214. doi: 10.1210/edrv.21.2.0394.

McKey J, Anbarci DN, Bunce C, Ontiveros AE, Behringer RR, Capel B. (2022). Integration of mouse ovary morphogenesis with developmental dynamics of the oviduct, ovarian ligaments, and rete ovarii. Elife 11, e81088. doi: 10.7554/eLife.81088.

Meinsohn MC, Smith OE, Bertolin K, Murphy BD. (2019). The Orphan Nuclear Receptors Steroidogenic Factor-1 and Liver Receptor Homolog-1: Structure, Regulation, and Essential

814 Roles in Mammalian Reproduction. Physiol Rev. 99, 1249-1279. doi:
815 10.1152/physrev.00019.2018.

816 Meinsohn MC, Hughes CHK, Estienne A, Saatcioglu HD, Pépin D, Duggavathi R, Murphy BD.
817 (2021a). A role for orphan nuclear receptor liver receptor homolog-1 (LRH-1, NR5A2) in
818 primordial follicle activation. Sci Rep. 11, 1079. doi: 10.1038/s41598-020-80178-4.

819 Meinsohn MC, Saatcioglu HD, Wei L, Li Y, Horn H, Chauvin M, Kano M, Nguyen NMP,
820 Nagykery N, Kashiwagi A, Samore WR, Wang D, Oliva E, Gao G, Morris ME, Donahoe PK,
821 Pepin D. (2021b). Single-Cell sequencing reveals suppressive transcriptional programs regulated
822 by MIS/AMH in neonatal ovaries. PNAS 118, 20. doi: 10.1073/pnas.2100920118.

823 Miura K, Murata C, Harikae K, Suzuki H, Kanai-Azuma M, Kurohmaru M, Tsunekawa N, Kanai
824 Y. (2017). Defects in the first wave of folliculogenesis in mouse XO ovaries. J Reprod Dev. 63,
825 333-338. doi: 10.1262/jrd.2017-033.

826 Miyabayashi K, Tokunaga K, Otake H, Baba T, Shima Y, Morohashi K. (2015). Heterogeneity of
827 ovarian theca and interstitial gland cells in mice. PLoS One. 10, e0128352. doi:
828 10.1371/journal.pone.0128352.

829 Mork L, Maatouk DM, McMahon JA, Guo JJ, Zhang P, McMahon AP, Capel B (2012).
830 Temporal differences in granulosa cell specification in the ovary reflect distinct follicle fates in
831 mice. Biol Reprod. 86, 37. doi: 10.1095/biolreprod.111.095208.

832 Morris ME, Meinsohn MC, Chauvin M, Saatcioglu HD, Kashiwagi A, Sicher NA, Nguyen N,
833 Yuan S, Stavely R, Hyun M, Donahoe PK, Sabatini BL, Pépin D. (2022). A single-cell atlas of
834 the cycling murine ovary. Elife 11, e77239. doi: 10.7554/eLife.77239.

835 Myers M, Britt KL, Wreford NG, Ebling FJ, Kerr JB. (2004). Methods for quantifying follicular
836 numbers within the mouse ovary. Reproduction. 127(5):569-80. doi: 10.1530/rep.1.00095.

837 Nelson JF, Karelus K, Felicio LS, Johnson TE (1990). Genetic influences on the timing of
838 puberty in mice. Biol Reprod. 42, 649-55. doi: 10.1095/biolreprod42.4.649.

839 Niu W, Spradling AC (2020). Two distinct pathways of pregranulosa cell differentiation support
840 follicle formation in the mouse ovary. Proc Natl Acad Sci U S A. 117, 20015-20026. doi:
841 10.1073/pnas.2005570117.

842 Niu W, Spradling AC. (2022). Mouse oocytes develop in cysts with the help of nurse cells. Cell
843 185, 2576-2590. doi: 10.1016/j.cell.2022.05.001.

844 Pazdernik N, Schedl T. (2013). Introduction to germ cell development in Caenorhabditis elegans.
845 Adv Exp Med Biol. 757:1-16. doi: 10.1007/978-1-4614-4015-4_1.

Richards JS, Ren YA, Candelaria N, Adams JE, Rajkovic A. (2017). Ovarian Follicular Theca Cell Recruitment, Differentiation, and Impact on Fertility. Endocr Rev. 39, 1-20. doi: 10.1210/er.2017-00164.

Schneider, M., Wolf, E., Hoeflich, A., & Lahm, H. (2002). IGF-binding protein-5: flexible player in the IGF system and effector on its own. Journal of Endocrinology, 172, 423-440.

Simerly RB. (2002). Wired for reproduction: organization and development of sexually dimorphic circuits in the mammalian forebrain. Annu Rev Neurosci. 25, 507-36. doi: 10.1146/annurev.neuro.25.112701.142745.

Sisk CL, Zehr JL. (2005). Pubertal hormones organize the adolescent brain and behavior. Front Neuroendocrinol. 26, 163-74. doi: 10.1016/j.yfrne.2005.10.003.

Templin JS, Wyrosdic JC, David CD, Wyrosdic BN, Lapp HE, Bala A, Bartlett A, Khan Z, Rokicki A, Park JH. (2019). Peripubertal gonadal steroids are necessary for steroid independent male sexual behavior in castrated B6D2F1 male mice. Horm Behav. 113, 38-46. doi: 10.1016/j.yhbeh.2019.04.013.

Trova S, Bovetti S, Bonzano S, De Marchis S, Peretto P. (2021). Sex Steroids and the Shaping of the Peripubertal Brain: The Sexual-Dimorphic Set-Up of Adult Neurogenesis. Int J Mol Sci. 22, 7984. doi: 10.3390/ijms22157984.

Viuff MH, Just J, Brun S, Dam TV, Hansen M, Melgaard L, Hougaard DM, Lappe M, Gravholt CH (2022). Women With Turner Syndrome Are Both Estrogen and Androgen Deficient: The Impact of Hormone Replacement Therapy. J Clin Endocrinol Metab. 107, 1983-1993. doi: 10.1210/clinem/dgac167.

Walters KA, Rodriguez Paris V, Aflatounian A, Handelsman DJ (2019). Androgens and ovarian function: translation from basic discovery research to clinical impact. J Endocrinol. 242, R23-R50. doi: 10.1530/JOE-19-0096.

Yoest KE, Henry MG, Velisek HA, Veenema AH. (2023). Development of social recognition ability in female rats: Effect of pubertal ovarian hormones. Horm Behav. 151, 105347. doi: 10.1016/j.yhbeh.2023.105347.

Zheng W, Zhang H, Gorre N, Risal S, Shen Y, Liu K (2014a). Two classes of ovarian primordial follicles exhibit distinct developmental dynamics and physiological functions. Hum Mol Genet. 23, 920-28. doi: 10.1093/hmg/ddt486.

Zheng W, Zhang H, Liu K (2014b). The two classes of primordial follicles in the mouse ovary: their development, physiological functions and implications for future research. Mol Hum Reprod. 20, 286-292. doi: 10.1093/molehr/gau007.

879 Zhou J, Jiang X, Wu H, Zhang L, Chen M, Chen M, Shen Z, Guo X, Wang H, Gao F. Dissecting
880 the fate of Foxl2-expressing cells in fetal ovary using lineage tracing and single-cell
881 transcriptomics. Cell Discov. 2022 Dec 27;8(1):139. doi: 10.1038/s41421-022-00492-1.

882 Zhou Y, Zhu W, Guo Z, Zhao Y, Song Z, Xiao J (2007). Effects of maternal nuclear genome on
883 the timing of puberty in mice offspring. J Endocrinol. 193, 405-12. doi: 10.1677/joe.1.07049.

884 Zhou Y, Zhou B, Pache L, Chang M, Khodabakhshi AH, Tanaseichuk O, Benner C, Chanda SK.
885 (2019). Metascape provides a biologist-oriented resource for the analysis of systems-level
886 datasets. Nat Commun. 10, 1523. doi: 10.1038/s41467-019-09234-6.

887 Zhu, C. H. and Xie, T. (2003). Clonal expansion of ovarian germline stem cells during niche
888 formation in Drosophila. Development 130, 2579-2588.

889 Zuckerman-Levin N, Frolova-Bishara T, Militianu D, Levin M, Aharon-Peretz J, Hochberg Z
890 (2009). Androgen replacement therapy in Turner syndrome: a pilot study. J Clin Endocrinol
891 Metab. 94, 4820-7. doi: 10.1210/jc.2009-0514.

892

893 FIGURE LEGENDS

894 **Figure 1**. Wave 1 follicles are remodeled prior to peri-puberty.

895 (**A**) Schematic diagrams of fetal and postnatal ovaries at the indicated stages (E = embryonic
896 day; P = postnatal day). Wave 1 follicles, located in the ovarian medulla (below the dashed line),
897 retain bipotential pre-granulosa cells (BPGs, green) and develop without delay. In contrast,
898 cortical follicles, which become quiescent primordial follicles (Wave 2), undergo replacement of
899 BPGs by epithelial pre-granulosa cells (EPGs, yellow). This replacement is completed by P5. By
900 P21 (3 wk), wave 1 follicles undergo atresia, characterized by oocyte loss. Germ cells or oocytes
901 are shown in blue. Developmental stages are indicated in the diagram. Dashed line: Medulla-
902 cortex boundary. (**B**) Postnatal follicular developmental timeline: Wave 1 antral follicles emerge
903 by 3 weeks (Figure S1A-C); Juvenile sexual development (peri-puberty) occurs at 4-5 weeks;
904 Puberty and ovulation take place around 7-8 weeks. (**C**) Annotation of total follicles in P5 and
905 P10 ovaries using Imaris software (gray balls). Each follicles with DDX4-postive oocyte was

906 manually counted and labeled using the Imaris spot model. Scale bars: left, 50 µm; right, 70 µm.
907 (**D**) Total follicle counts in P5 and P10 ovaries (mean ± SD; N = 3-4). ns, not significant. (**E**)
908 Annotation of wave 1 follicles in P5 and P10 ovaries using Imaris software (gray balls). Follicles
909 with oocytes larger than 20 µm in diameter, primarily located in the medulla, are classified as
910 wave 1 follicles at the indicated times. Each gray ball represents one follicle. Scale bars: left, 50
911 µm; right, 70 µm. (**F**) Wave 1 follicle counts in P5 and P10 ovaries (mean ± SD; N = 3-4). ns,
912 not significant. (**G**) 3D projection of the ovary at P14, reconstructed using the Imaris surface
913 model. Scale bars = 50 µm. (**H**) Oocyte volume increase in wave 1 follicles over time (mean ±
914 SD; N = 10). (Note: Nuclear volume is excluded, as DDX4 is a cytoplasmic protein.). ****$p <$
915 0.0001. (**I**) Representative images of ovary at 4 wk and 5 wk. Left (4 wk): arrowheads indicate
916 an atretic follicle with a distorted oocyte and disorganized granulosa cells; arrow points to a
917 developing healthy secondary follicle. Right (5 wk): arrowheads indicate degrading follicles at
918 various stages; arrow points to a developing healthy secondary follicle. Scale bars = 100 µm. (**J**)
919 Wave 1 follicle remodeling, indicated by oocyte loss over time (mean ± SD; N = 3-4). Oocyte
920 loss begins around 3 wk and continues through 5 wk, accompanied by granulosa cell
921 disorganization and cell death. ns, not significant; ** $p < 0.01$; ****$p < 0.0001$.

922 **Figure supplement 1**. Wave 1 follicle development in the early juvenile ovary.

923 **Figure supplement 2**. Wave 1 follicles begin to remodel by 3 weeks.

924

925 **Figure 2**. Wave 1 follicles lose granulosa cells during remodeling.

926 (**A**) Schematic diagram illustrating the activation of *Foxl2*-driven EYFP expression following
927 TAM injection at E16.5. TAM administration at E16.5 induces the excision of a stop cassette,

928 leading to EYFP expression in granulosa cells of follicles (see Methods). (**B**) Efficient EYFP
929 labeling of granulosa cells in wave 1 medullary follicles of a 2-week ovary following TAM
930 injection at E16.5, as shown in (A), magnified in the right. Scale bars: left, 100 µm; right, 30 µm.
931 (**C**) EYFP-labeled follicles that have reached the primary/secondary follicle stage by 2 weeks are
932 quantified using Imaris software, with annotation performed using the spot model. Left: A
933 section showing annotated labeled follicles (white circles). Right: 3D projection using Imaris
934 software, where labeled follicles are represented by gray spheres. Scale bars: left, 100 µm; right,
935 80 µm. (**D**) By 5 wk, EYFP-labeled follicles that have reached the preantral/antral follicle stage
936 are quantified using Imaris software and annotated with the spot function. Left: A section
937 showing annotated labeled follicles (white circles). Right: 3D projection using Imaris software,
938 with labeled follicles represented by gray spheres. Scale bars = 200 µm. (**E**) Over 90% of wave 1
939 follicles contained EYFP-positive granulosa cells at 2 wk. At 5 wk, approximately 70% of
940 normal antral follicles contained EYFP-positive granulosa cells. (**F**) Quantification of wave 1
941 follicle numbers (representative images shown in C-D) shows a decline from 2 to 5 weeks.
942 ****$p < 0.0001$. Each dot represents one sample. (**G**) Representative section from a 5-week
943 ovary reveals ongoing remodeling of wave 1 follicles. Follicles near the medullary core appear
944 small and without oocytes (arrowheads), with few remaining EYFP-labeled granulosa cells, as
945 seen in the follicle boxed in "1" and enlarged in G'. In contrast, a normal antral follicle in
946 rectangle "2" enlarged in G", contains numerous EYFP-labeled granulosa cells. Right: The
947 average number of EYFP-labeled granulosa cells in medullary follicles before remodeling (3
948 weeks) is compared to remodeled medullary follicles at 5 weeks. Each point represents one
949 analyzed follicle. ****$p < 0.0001$. Scale bars: left, 200 µm; right, 50 µm. (**H**) About 80% of
950 remodeled follicles still retain some EYFP-labeled granulosa cells at 5 wk, consistent with their

951 wave 1 origin. Dashed line: follicle boundary; arrowheads: EYFP-positive granulosa cells. Each
952 point represents one analyzed follicle. (**I**) Remnant granulosa cells of remodeled wave 1 follicles
953 continue to express Foxl2 at 5 weeks. TAM was injected into Foxl2-CreERT2; R26R-LSL-
954 tdTomato mice at 5 weeks, and ovaries were collected one week later. Arrowheads indicate
955 remodeled follicles, with one remodeled follicle (outlined in the rectangle) enlarged on the right.
956 Scale bars: left, 100 μm; right, 20 μm.

957 **Figure supplement 3**. Lineage labeling using Foxl2-CreERT2 and R26R-LSL-tdTomato

958

959 **Figure 3**. The labeling and quantification of boundary follicles

960 (**A**) At 2 wk, one or more granulosa cells in some primordial follicles located at the medulla-
961 cortex boundary are labeled with EYFP (enlarged in "1", "2", "3") following TAM injection, as
962 shown in the schematic. These follicles are referred to as boundary follicles or, in accordance
963 with the wave classification, wave 1.5 follicles. Dash line, medulla-cortex boundary. Scale bars:
964 left, 100 μm; right, 20 μm. (**B**) Quantification shows that 7% (421 ± 74) of the total 5,843 ±
965 1,256 primordial follicles contained EYFP-labeled granulosa cells in the labeled experiment
966 shown in (A). Each point represents one analyzed sample. Labeled PFs: Labeled primordial
967 follicles. (**C**) Representative images of *Foxl2-CreERT2; R26R-LSL-EYFP* mouse ovary injected
968 with TAM at E14.5. Boundary follicles labeled with EYFP are enlarged on the right. Dash line
969 indicates the medulla-cortex boundary. Scale bars: left, 100 μm; right, 20 μm. (**D**) Approximately
970 70% of secondary follicles in 5 wk ovaries contain EYFP-labeled granulosa cells, suggesting
971 they originate from labeled primordial follicles (wave 1.5) at 2 wk. TAM was injected at E16.5.
972 Each point represents one analyzed sample. Scale bar = 50 μm.

973

974

975 **Figure 4**. Follicles remodel to form an interconnected stromal network rich in thecal secretory

976 cells.

977 (**A**) Schematic diagram illustrating lineage labeling of *Cyp17a1*-expressing theca cells,

978 interstitial gland cells, and potentially other cell types using *Cyp17a1*-iCre; *R26R-LSL-tdTomato*

979 mouse model. (**B**) 2 wk ovary showing tdTomato-labeled theca cells sheathing follicles

980 (arrowhead) and putative interstitial gland cells between follicles (rectangle). Scale bars: left, 20

981 µm; right, 5 µm. (**C**) 3D reconstruction of follicles with surrounding labeled theca cells and

982 interconnected interstitial gland cells in a 2 wk ovary. Left: 3D projection using Imaris software.

983 Right: Pseudo-color annotation using the Imaris surface model. Green: Oocytes. Red: *Cyp17a1*-

984 expressing cells, including theca and interstitial gland cells. Scale bars = 20 µm. (**D-E**)

985 Representative images of 2wk (D) and 5 wk (E) ovaries showing a dramatic increase in labeled

986 theca, interstitial, and possibly other Cyp17a1-lineage cells in the ovarian medulla. Scale bars =

987 100 µm. (**F-G**) Oil Red O staining (red) reveals a significant increase in lipid droplet storage in

988 ovarian medullary cells from 2 wk (F) to 5 wk (G) ovaries. Scale bars = 100 µm. (**H**)

989 Immunofluorescence staining of HSD3B1 and PLIN1 at 5 wk shows that genes required for

990 steroidogenesis and lipid droplet storage are highly expressed in medullary cells. Scale bars = 50

991 µm. (**I**) Electron microscopy of a remodeled follicle reveals cells with abundant lipid droplets

992 (LD) and characteristic mitochondria (mt) (boxed region magnified in right panel). Scale bar =

993 10 µm. (**J**) 3D reconstruction of a 5 wk ovary labeled by tdTomato expression activated by

994 *Cyp17a1-iCre*. Left: 3D projection using Imaris software. Right: Pseudo-color annotation using

995 the Imaris surface model. Red: Thecal/interstitial network structure. Balls: Oocyte locations.
996 Scale bars = 100 μm.

997 **Figure supplement 4**. Expansion of theca cells and its related cells - interstitial gland
998 population.

999

1000

1001 **Figure 5**. Single-cell RNA sequencing of 2 wk-6 wk ovaries

1002 (**A**) UMAP plot of ovaries from 2 wk to 6 wk, showing 31 initial clusters (c0-c30) represented in
1003 different colors. Sequencing data from different ages were merged before summit to Seurat.
1004 (detailed information in the methods section). (**B**) The ovarian cells from 2 wk to 6 wk contribute
1005 to almost every cluster in the UMAP plot. O2w: scRNA sequencing data from 2 wk ovary. O3w:
1006 3 wk ovary. O4w: 4 wk ovary. O5w: 5 wk ovary. O6w: 6 wk ovary. (**C**) The cell type groups are
1007 indicated by colored regions, with their relationship to the numbered initial clusters as shown in
1008 A. Granulosa cells: c1, c2, c3, c5, c10, c12, c20, c21, c24 and c30; Stromal cells: c0, c4, c7, c8,
1009 c9, 13, c17 and c19; Theca cells: c16; Hematopoietic cells: c23; Endothelial cells: c22 and c27;
1010 Pericytes: c18; Smooth muscle cells: c26; Epithelial cells: c25 and c28; Low UMI: c6, c11, c15
1011 and c29; TBD (To be determined): c14. (**D**) Multiviolin plot of selected marker gene expression
1012 across different cell types. Y-axis: Gene names with expression levels normalized for display. X-
1013 axis: Cell types.

1014

1015 **Figure 6**. Further re-cluster analysis of sequencing data.

1016 (**A**) UMAP plot of re-clustered granulosa cells from Figure 5A, showing 18 clusters (gc0-gc17).
1017 (**B**) The deduced ovarian follicle developmental stages are labeled and indicated by colored
1018 regions with their relationship to the numbered clusters shown in A. Primordial: gc11; Primary:
1019 gc3 and gc8; Secondary: gc1, gc4 and gc9; Antral: gc2, gc7, gc10 and gc13; Remodeling: gc0
1020 and gc6; Mitotic: gc5, gc12, gc14, gc15, gc16 and gc17. (**C**) Dot plot of marker gene expression
1021 in granulosa cells across different follicle stages. Y-axis: Cell types. X-axis: Gene names with
1022 expression levels normalized for display. (**D**) Pseudotime trajectory analysis using Monocle3
1023 reveals two pathway in secondary follicles: Path 1 leads to further development into antral
1024 follicles, while Path 2 results in remodeling follicles. (**E**) UMAP plot of re-clustered theca cell
1025 and stromal cells Figure 5A, showing 21 clusters (g0-g20). (**F**) The deduced mesodermal cell
1026 subgroups are labeled and indicated by colored regions and their relationship to the numbered
1027 clusters shown in panel E. Hoxd9+: g0; Tagln+: g1, g8, g14 and g17; Early TCs: g2 and g11;
1028 Late TCs: g9; Cxcl12+: g3, g5 and g20; Cd24a+: g4; Col11a1+: g6 and g7; Col14a1+: g10 and
1029 g19; Mitotic: g12, g13, g15 and g18; TBD (To be determined): g16. (G) Diagram of
1030 steroidogenic gene expression in theca and granulosa cells and their role in androgen and
1031 estrogen synthesis. Top panel: The diagram illustrates the synthesize of androgen in theca cells
1032 and estrogen in granulosa cells from cholesterol. Bottom panel: The estimated numbers of
1033 steroidogenic theca cells expressing three key steroidogenesis genes in the sequencing data—
1034 *Cyp11a1*, *Hsd3b1*, and *Cyp17a1*—are shown, along with those expressing all four essential
1035 genes (*Cyp11a1*, *Hsd3b1*, *Cyp17a1*, and *Star*). The total cell number are shown in the first row.
1036 From 2 wk to 5 wk, the theca cell population increases, followed by a decline at 6 weeks.
1037 Meanwhile, the number and percentage of theca cells expressing all four essential genes
1038 progressively increase. In contrast, the estimated numbers of granulosa cells expressing *Hsd3b1*,

1039 *Hsd17b1*, and *Cyp19a1* follow a fluctuating pattern, decreasing from 2wk to 4 wk before rising
1040 again at 5 wk. Notably, 2 wk corresponds to the time of minipuberty. (H) Estimated numbers of
1041 granulosa cells in follicles across developmental subclasses: primordial, primary, secondary,
1042 antral, remodeling, and mitotic cycling.

1043 **Figure supplement 5**. Analysis of single-cell RNA sequencing.

1044 **Figure supplement 6**. Analysis of other cell types.

1045 **Figure supplement 7**. Hormone receptor expression and XO mouse line.

1046

1047 **Figure 7**. Model of wave 1 follicle development and function.

1048 Wave 1 follicles undergo remodeling during the peri-pubertal period to expand the population of
1049 androgen-producing theca and interstitial cells. Gradients between the medulla and cortex
1050 facilitate the sequential activation of primordial follicles, a process that continues into early
1051 adulthood. We refer to these sequentially activated follicles as boundary follicles (Wave 1.5).
1052 These follicles, whose granulosa cells are derived from bipotential pre-granulosa cells (BPGs),
1053 remain dormant in the medulla and cortex until recruiting signals—either positive or negative—
1054 become available. Boundary follicles are typically recruited around 2 weeks of age and constitute
1055 the majority of developing follicles by 5 weeks. In parallel, wave 1 follicles remodel to support
1056 androgen production through their remaining theca cells and associated interstitial glands.

1057

1058

1059

1060 Table 1. Summary of whole mount C57BL/6J ovary analyses

Postnatal age	Total follicles/ ovary	Antral	Wave 1 follicles/ovary	Reference files	Ovaries analyzed
P5-7	3822 +/- 838	0	278 +/- 17	1wk_1.mp4; 1wk_2.mp4	4
P10-P14	3304 +/- 926	0	293 +/- 36	2wk_1.mp4; 2wk_2.mp4	3
3 wk	3089 +/- 669	23 +/- 2	ND	3wk_1.mp4 3wk_2.mp4	3
4 wk	ND	35 +/- 2	ND	4wk_1.mp4 4wk_2.mp4	4
5 wk	ND	24 +/- 4	ND	5wk_1.mp4 5wk_2.mp4	5

1061 Numbers are mean and standard deviation.

Fig. 1

A

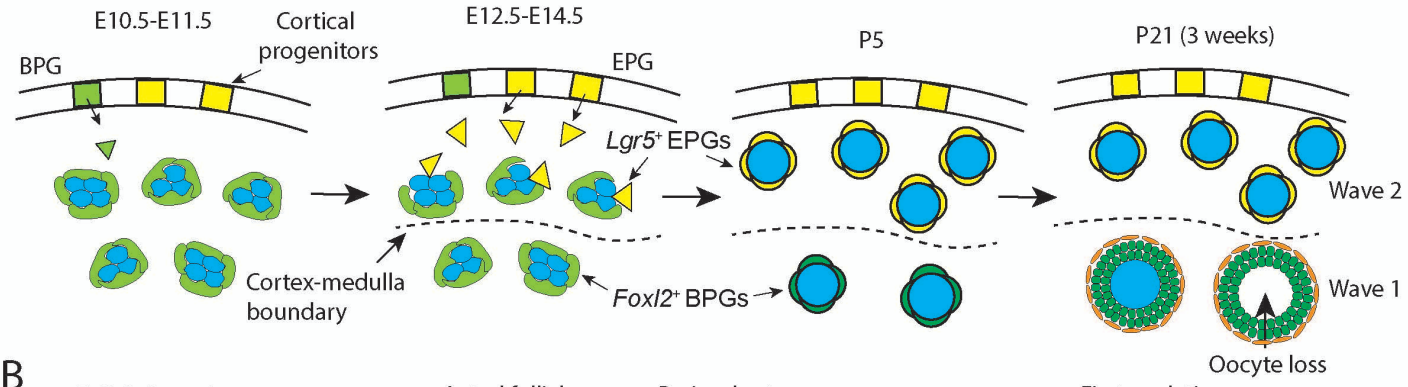

B

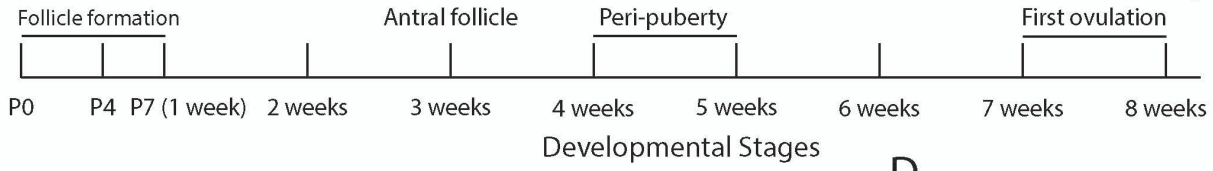

C

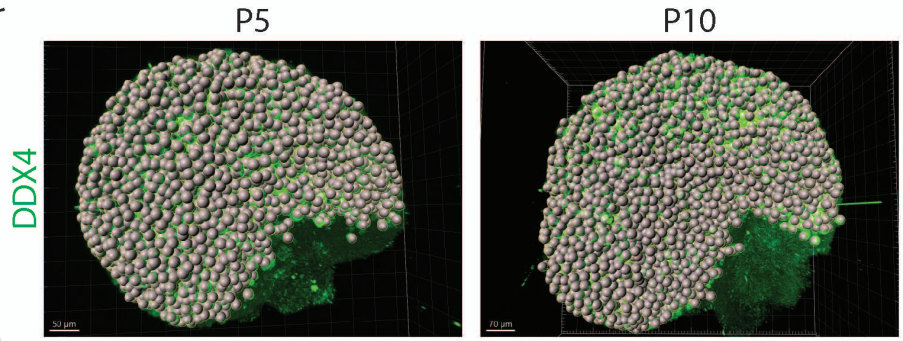

D

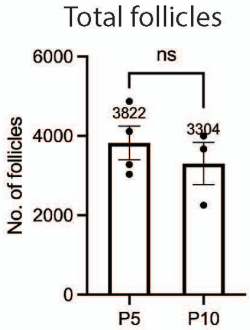

E

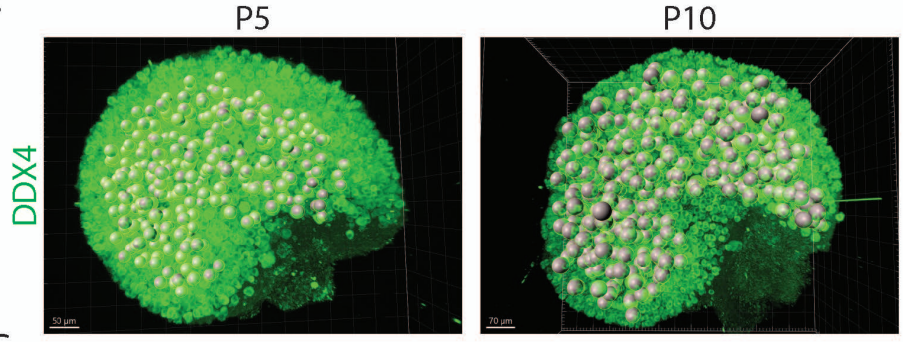

F

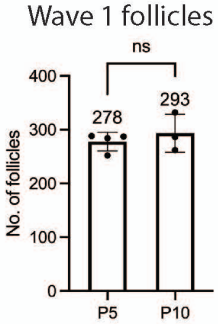

G

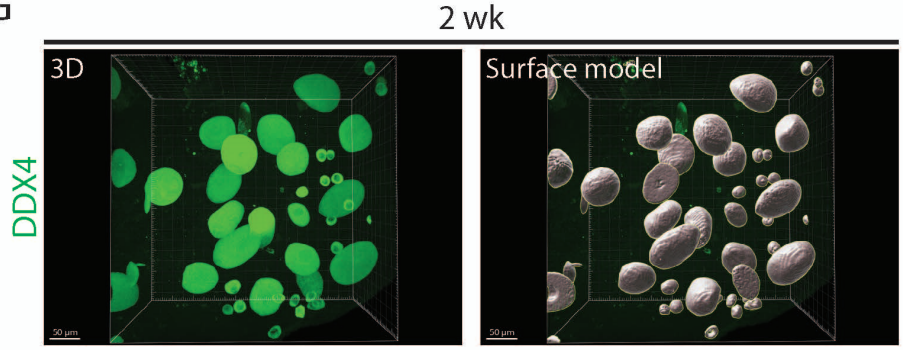

H

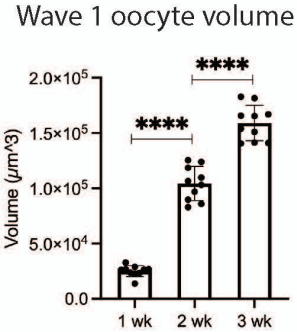

I

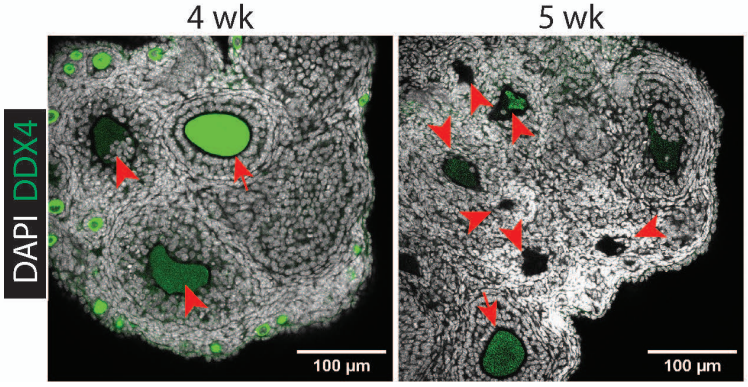

J

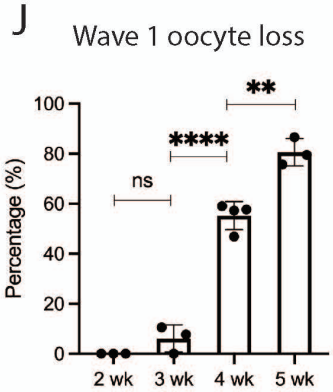

Fig. 2

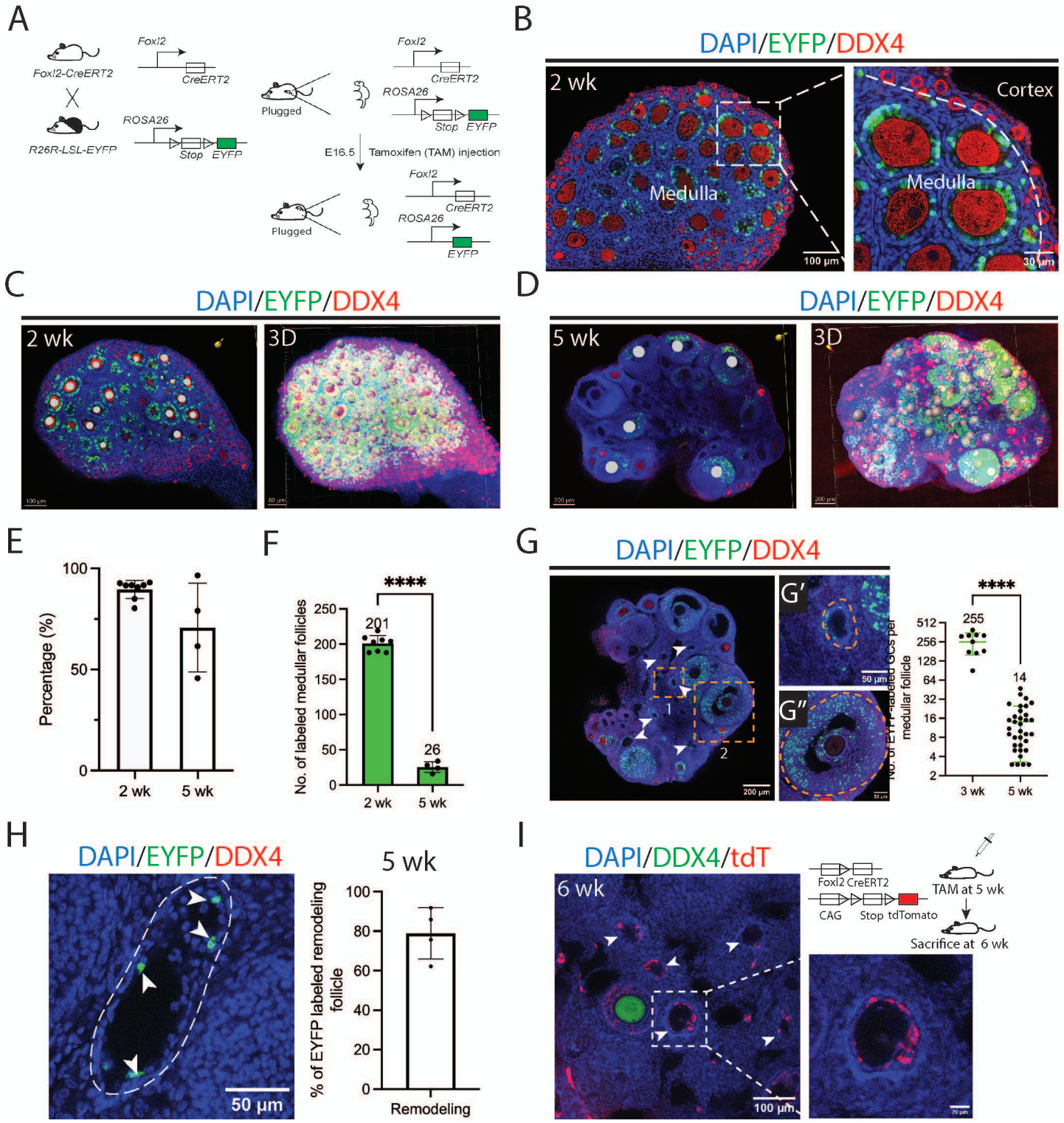
A
Foxl2-CreERT2
R26R-LSL-EYFP
Foxl2
CreERT2
ROSA26
Stop
EYFP
Plugged
E16.5
Tamoxifen (TAM) injection
B
DAPI/EYFP/DDX4
2 wk
Medulla
Cortex
100 µm
30 µm
C
DAPI/EYFP/DDX4
2 wk
3D
D
DAPI/EYFP/DDX4
5 wk
3D
E
Percentage (%)
2 wk
5 wk
F
No. of labeled medullar follicles
****
201
26
G
DAPI/EYFP/DDX4
G′
G″
1
2
200 µm
50 µm
No. of EYFP-labeled OCs per medullar follicle
255
14
3 wk
5 wk
H
DAPI/EYFP/DDX4
50 µm
5 wk
% of EYFP labeled remodeling follicle
Remodeling
I
DAPI/DDX4/tdT
6 wk
100 µm
Foxl2 CreERT2
CAG
Stop tdTomato
TAM at 5 wk
Sacrifice at 6 wk

Fig. 3

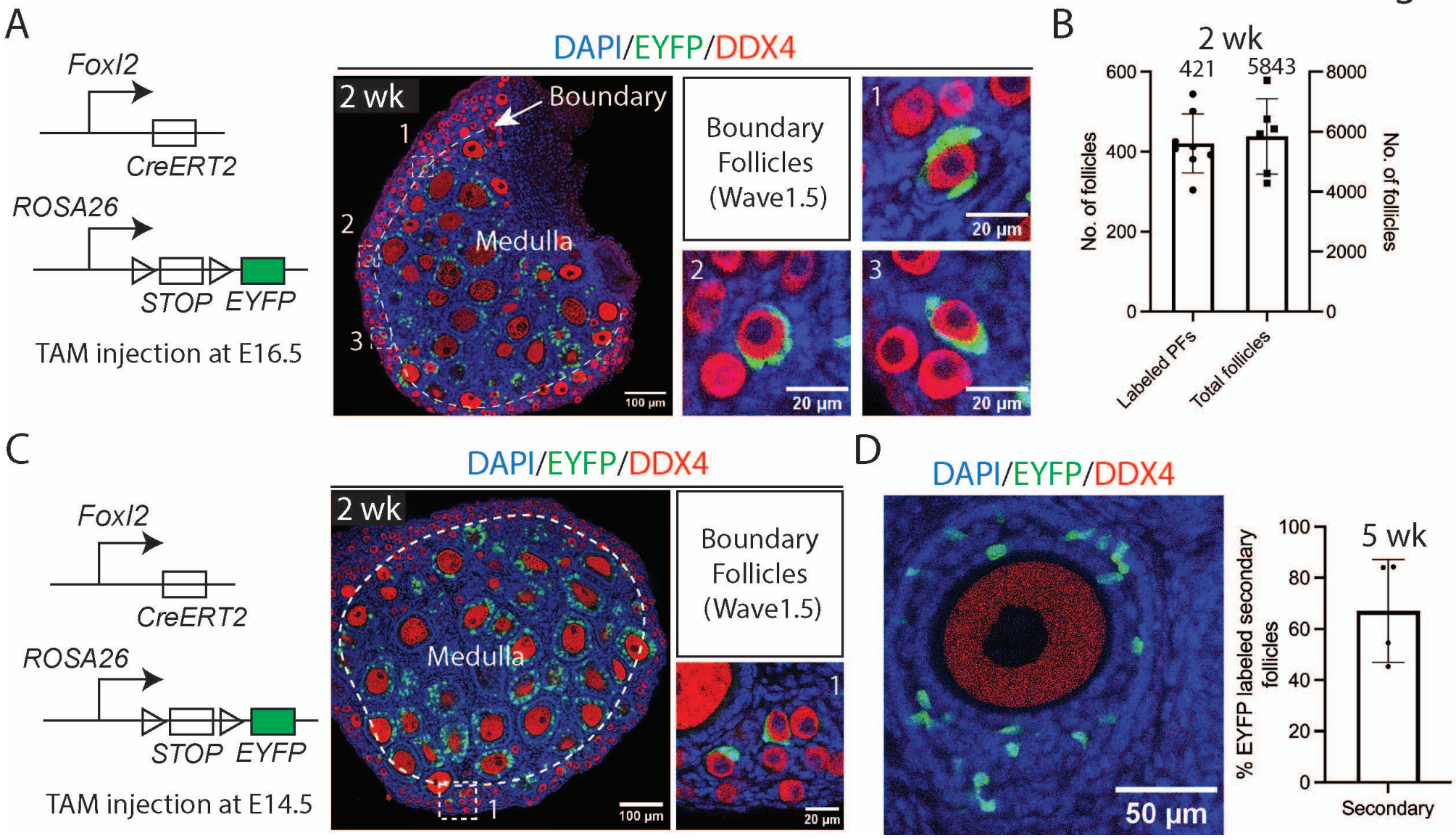
A
Foxl2
CreERT2
ROSA26
STOP EYFP
TAM injection at E16.5
DAPI/EYFP/DDX4
2 wk
Boundary
Medulla
1
2
3
100 µm
Boundary Follicles (Wave1.5)
20 µm
B
2 wk
421
5843
No. of follicles
600
400
200
0
8000
6000
4000
2000
Labeled PFs
Total follicles
C
Foxl2
CreERT2
ROSA26
STOP EYFP
TAM injection at E14.5
DAPI/EYFP/DDX4
2 wk
Medulla
Boundary Follicles (Wave1.5)
D
DAPI/EYFP/DDX4
50 µm
% EYFP labeled secondary follicles
5 wk
100
80
60
40
20
0
Secondary

Fig. 4

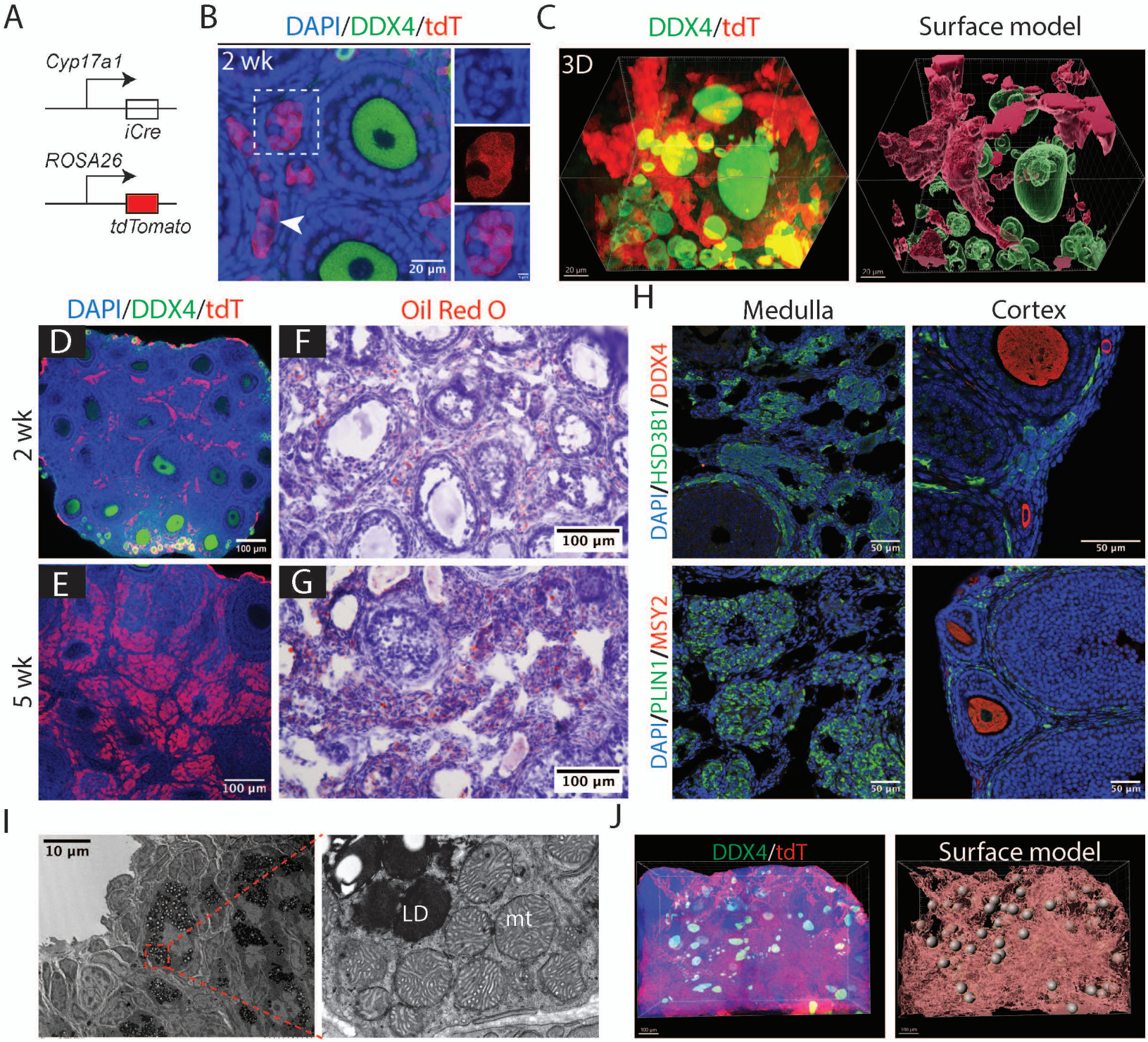
A
Cyp17a1
iCre
ROSA26
tdTomato
B
DAPI/DDX4/tdT
2 wk
20 µm
C
DDX4/tdT
3D
Surface model
DAPI/DDX4/tdT
Oil Red O
D
E
F
G
2 wk
5 wk
100 µm
H
Medulla
Cortex
DAPI/HSD3B1/DDX4
DAPI/PLIN1/MSY2
50 µm
I
10 µm
LD
mt
J
DDX4/tdT
Surface model

Fig. 5

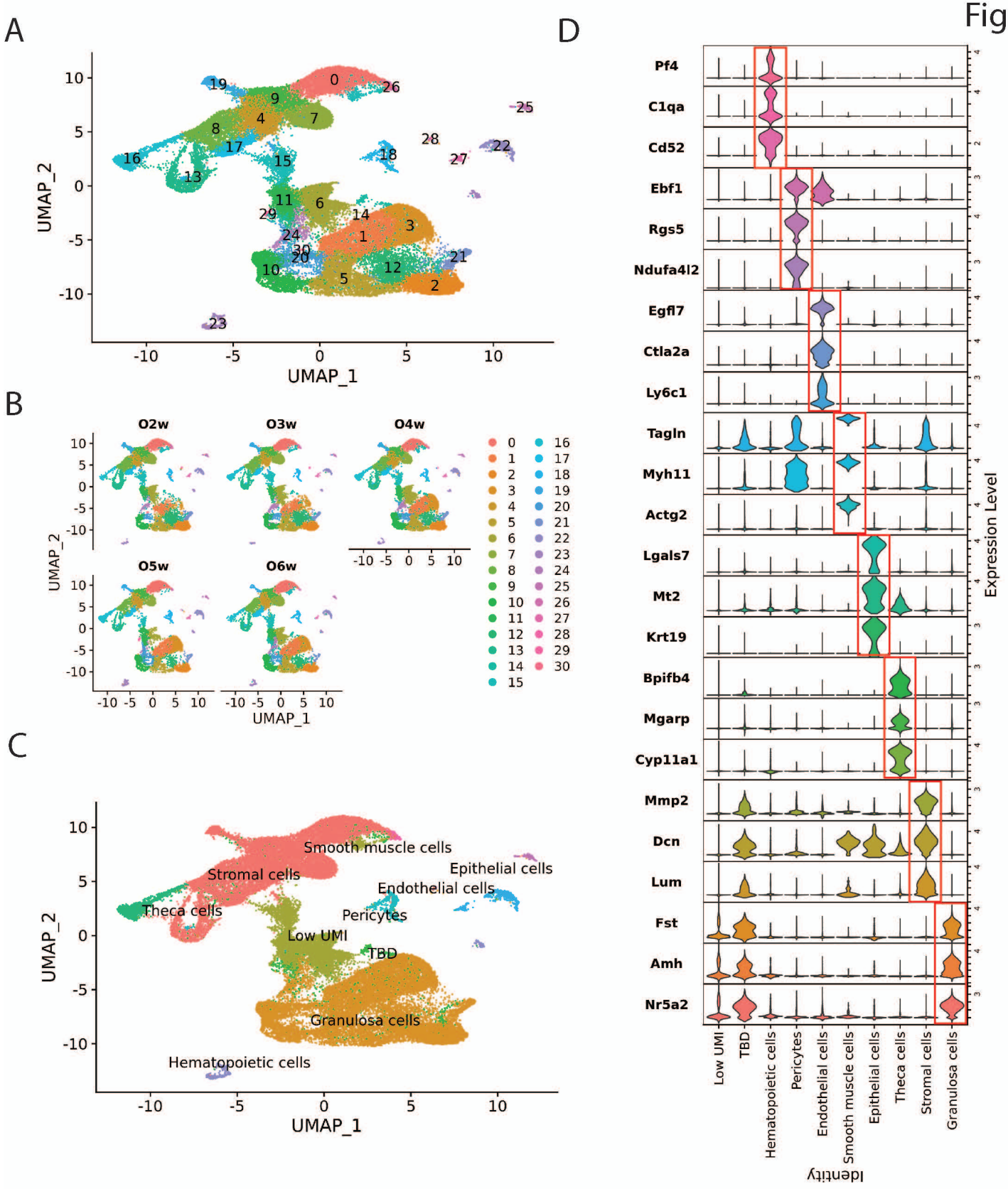
A
UMAP_2
UMAP_1
B
O2w
O3w
O4w
O5w
O6w
C
Smooth muscle cells
Epithelial cells
Stromal cells
Endothelial cells
Theca cells
Pericytes
Low UMI
TBD
Granulosa cells
Hematopoietic cells
D
Pf4
C1qa
Cd52
Ebf1
Rgs5
Ndufa4l2
Egfl7
Ctla2a
Ly6c1
Tagln
Myh11
Actg2
Lgals7
Mt2
Krt19
Bpifb4
Mgarp
Cyp11a1
Mmp2
Dcn
Lum
Fst
Amh
Nr5a2
Expression Level
Identity
Low UMI
TBD
Hematopoietic cells
Pericytes
Endothelial cells
Smooth muscle cells
Epithelial cells
Theca cells
Stromal cells
Granulosa cells

Fig. 6

A

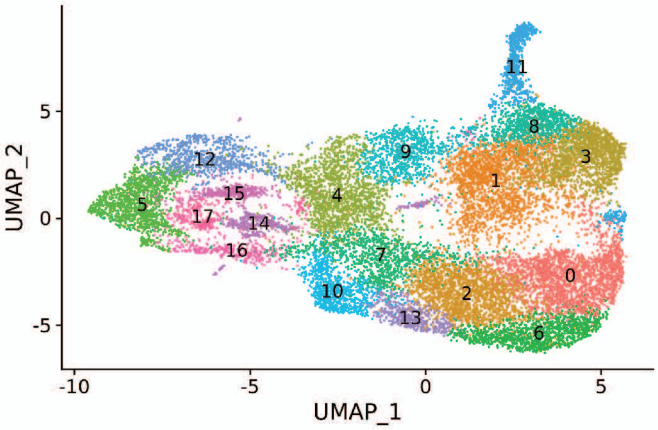

B

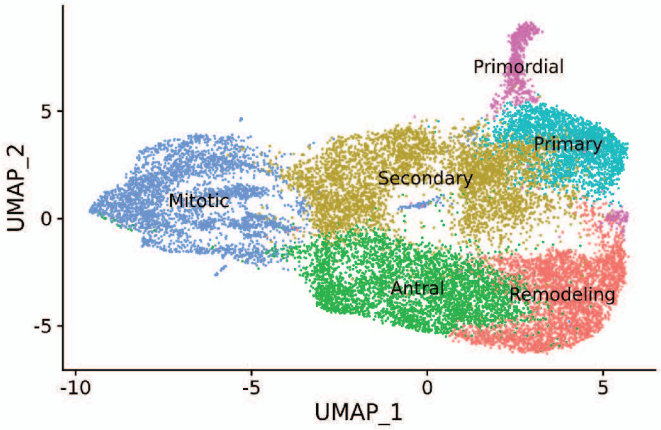

C

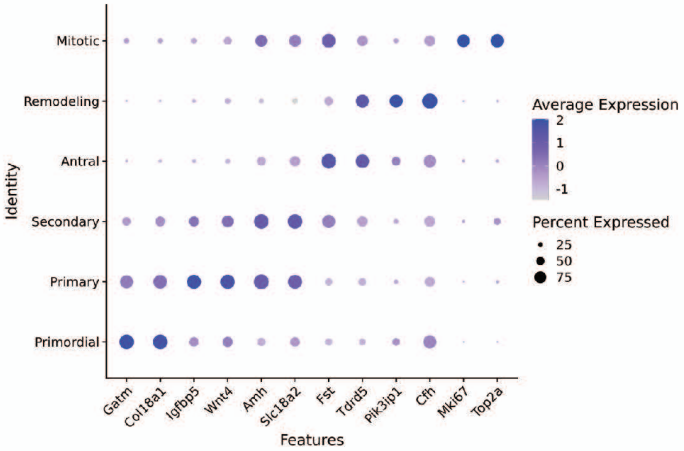

D

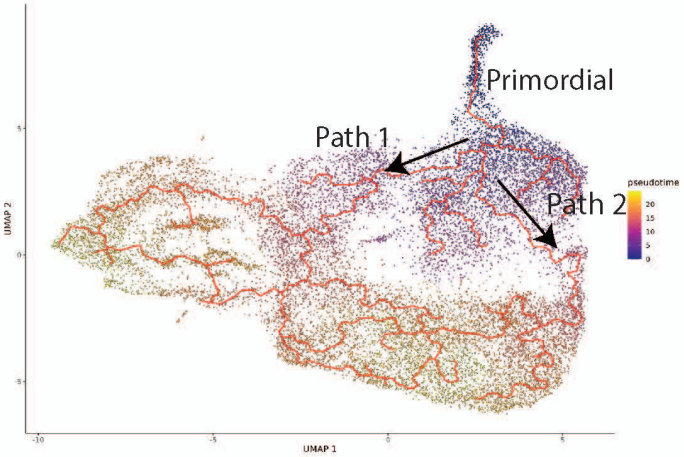

E

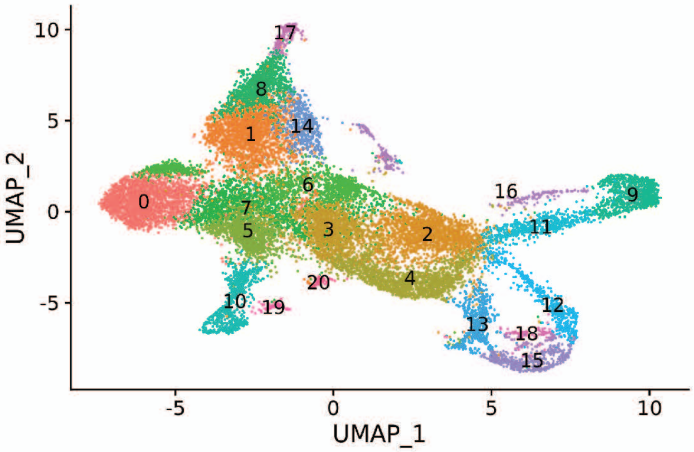

F

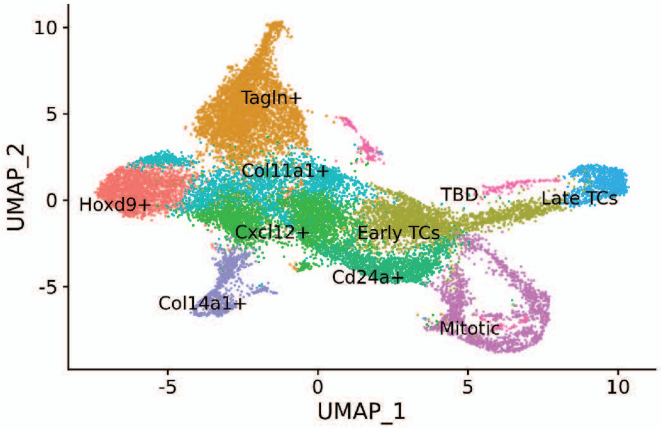

G

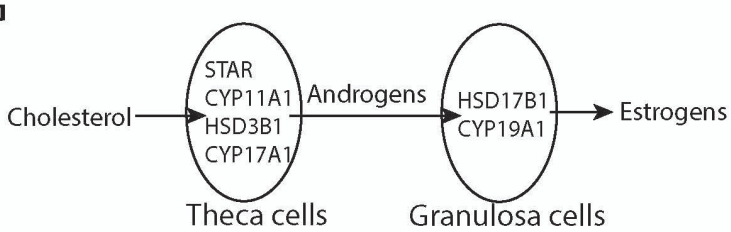

		2 wk (9471)	3 wk (9253)	4 wk (11077)	5 wk (7779)	6 wk (10583)
Theca cells	Cyp11a1 &Hsd3b1 &Cyp17a1	96	75	147	633	89
	Cyp11a1 &Hsd3b1 &Cyp17a1 &Star	41 (42.7%)	32 (42.7%)	72 (49.0%)	526 (83.1%)	29 (32.6%)
Granulosa cells	Hsd3b1 &Hsd17b1 &Cyp19a1	247	202	68	238	626

H

	2 wk	3 wk	4 wk	5 wk	6 wk
Primordial	316	206	124	81	81
Primary	794	742	392	230	365
Secondary	1086	1131	896	442	760
Antral	356	587	1416	590	1050
Remodeling	77	138	1348	766	910
Mitotic cycling	478	647	1072	620	749

Fig. 7

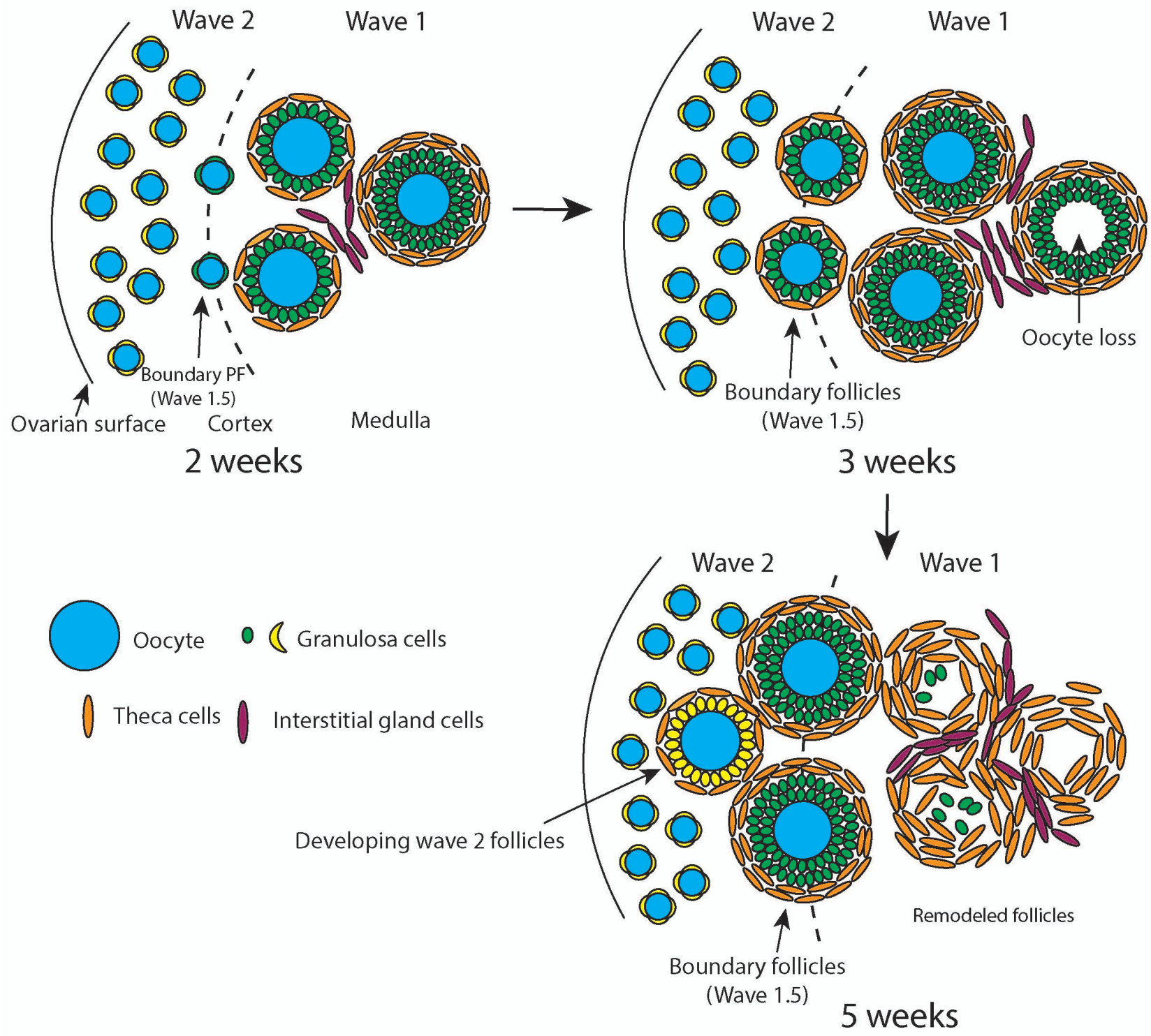
Wave 2
Wave 1
Boundary PF
(Wave 1.5)
Ovarian surface
Cortex
Medulla
2 weeks
Wave 2
Wave 1
Oocyte loss
Boundary follicles
(Wave 1.5)
3 weeks
Oocyte
Granulosa cells
Theca cells
Interstitial gland cells
Wave 2
Wave 1
Developing wave 2 follicles
Remodeled follicles
Boundary follicles
(Wave 1.5)
5 weeks

1062 # Supplemental Figure Legends

1063 **Figure supplement 1**. Wave 1 follicle development in the early juvenile ovary.

1064 (**A-D**) Representative images of wave 1 follicles stained for DDX4 (green) at P5, P7, P14 (2 wk),
1065 and P21 (3 wk). A: Early primary follicle with theca cells (arrow); B: Late primary follicle; C:
1066 Secondary follicle; D: Antral follicle. White arrowhead: non-surrounded nucleus; Red
1067 arrowhead: Pyknotic nuclei of granulosa cells. Scale bars in, A: 20 µm; others: 50 µm.

1068

1069 **Figure supplement 2**. Wave 1 follicles begin to remodel by 3 weeks.

1070 (**A**) Electron microscopy of follicles at 5 wk ovary. Left: Normal follicle. Middle: intermediate
1071 follicle, in which the oocyte cytoplasm shrinks and begins degrade, indicated by the space
1072 between the oocyte and ZP, the absence of microvilli, and folding of the ZP (red arrow). Right:
1073 Remodeled follicle, where the oocyte has disappeared but the ZP remains. Surrounding theca and
1074 interstitial gland cells further accumulate lipid droplets. The boxed region is magnified in the
1075 lower panel. Abbreviations: Oo = oocyte; ZP = zona pellucida; LD = lipid droplet; mt =
1076 mitochondria; mv = microvilli. Scale bars = 20 µm. (**B**) DAPI-stained DBA/2J ovaries showing
1077 remodeling wave 1 follicles (arrowheads) and normally developing follicles (arrows). Left (3
1078 wk): Early remodeling follicles are observed in the central medulla (arrowheads). Right (7 wk):
1079 Wave 1 follicle derivatives retain an empty shape (arrowheads), remaining visible alongside
1080 normal follicles (arrows) and corpora lutea (asterisks). Ovaries were stained and imaged as
1081 whole mounts; only a single section is shown here. Scale bars = 200 µm.

1082

1083 **Figure supplement 3**. Lineage labeling using *Foxl2-CreERT2* and *R26R-LSL-tdTomato*

1084 (**A**) Schematic diagram of the experiment. The *Foxl2-CreERT2* mouse line was generated with
1085 EGFP inserted into the *Foxl2* locus, resulting in weak EGFP signal detectable in the cytoplasm

1086 using an EGFP antibody. To rule out the possibility that the observed signal originated from the
1087 *Foxl2* locus rather than *ROSA26-EYFP*, we repeated the experiment using the *Foxl2-CreERT2;*
1088 *R26R-LSL-tdTomato* mouse line. (**B**) At 2 wk, wave 1 follicle are labeled. By 5 wk, ome have
1089 turned over, as indicated by cavities left by disappeared oocytes and remaining tdTomato signals
1090 (arrowheads), while others have developed into antral follicles (arrow). One developing early
1091 primary follicle in the boxed region is shown in panel C. Scale bars are included in the images.
1092 (**C**) The EGFP channel shows a weak cytoplasmic signal from the Foxl2 locus, distinct from the
1093 strong, evenly distributed expression of EYFP from the *ROSA-EYFP* reporter shown in Figure
1094 3/4. Scale bar, 20 µm. (**D**) Boundary follicles (enlarged on the right) were observed in the 2 wk
1095 ovary of *Foxl2-CreERT2; R26R-LSL-tdTomato* mouse line injected with TAM at E16.5. Scale
1096 bars: left, 50 µm; right: 10 µm.
1097
1098 **Figure supplement 4**. Expansion of theca cells and its related cells - interstitial gland
1099 population.
1100 (**A**) Immunofluorescence staining of CYP17A1 protein in the ovary shows a significant increase
1101 of theca cells and interstitial gland within the stroma from 3 wk to 5 wwk. Scale bars = 50 µm.
1102 (**B**) Immunofluorescence staining of *Cyp17a1* lineage-traced ovary at 2 wk shows initial
1103 expression in theca cells and associated cells resembling interstitial gland cells (arrowheads).
1104 Additionally, a few granulosa cells were labeled (arrows), as previously reported (Bridges et al.,
1105 2008). Scale bar = 50 µm. (**C**) Structurally, steroidogenic theca cells closely resemble interstitial
1106 gland cells. In the electron microscopy images, red lines delineate distinct zones enriched in
1107 interstitial gland cells (1), theca cells (2), and granulosa cells (3), with each region magnified
1108 below. Zone 1 (rectangle labeled "1") represents interstitial gland cells. Zone 2 (rectangle labeled
1109 "2") contains steroidogenic theca cells. Zone 3 (rectangle labeled "3") corresponds to granulosa

1110 cells. Abbreviations: nu – nucleus; LD – lipid droplet; mt – mitochondria. Scale bars are
1111 included in the images. (**D**) *Cyp17a1* lineage-traced ovary at 4 wk and 7 wk shows a marked
1112 increase in the number of labeled theca cells and interstitial gland cells by 7 weeks. Extensive
1113 signal is also observed in the rete ovarii (arrowhead), indicating Cyp17a1 expression, as well as
1114 in the ovarian epithelium (arrow). Scale bars = 200 µm.
1115
1116 **Figure supplement 5**. Analysis of single-cell RNA sequencing
1117 (**A**) nFeature_RNA of the scRNA-seq data shows that clusers 6, 11, 15, 29 have low UMI. (**B**)
1118 Highlighting cluster 14 reveals its dispersed distribution. (**C**) The distribution of samples across
1119 clusters shows that cells from each sample contribute to all clusters (orig.ident). (**D**) Feature plot
1120 of marker gene expression from the reanalysis of mesenchymal cells, including late theca cells
1121 (*Cyp11a1*), early theca cells (*Hhip*), Tagln+ fibroblasts (*Tagln*), Hox9+ fibroblasts (*Hox9*),
1122 Col11a1+ fibroblasts (*Col11a1*), Cxcl12+ fibroblast (*Cxcl12*), Col14a1+ fibroblasts (*Col14a1*),
1123 Cd24a+ fibroblasts (*Cd24a*) and mitotic cells (*Mki67*).
1124
1125 **Figure supplement 6**. Analysis of other cell types
1126 (**A**) Expression plot of representative genes highly expressed in cluster 22, identified as
1127 endothelial cells in blood vessels, including *Esam*, *Flt1*, and *Cd93*. Red boxes in the top panel
1128 are enlarged in the bottom panel. cluster 27: Endothelial cells from lymphatic vessels. (**B**)
1129 Expression plot of representative genes highly expressed in cluster 27, identified as endothelial
1130 cells in lymphatic vessels, including *Ccl21a*, *Lyve1*, and *Prox1*. Red boxes in the top panel are
1131 enlarged in the bottom panel. (**C**) Expression plot of representative genes shared between
1132 pericytes and endothelial cells, including *Ebf1*, *Emid1*, and *Apold1*. Red boxes in the top panel
1133 are enlarged in the bottom panel. (**D**) Ridge plot of representative gene expression in epithelial

1134 cells from the ovarian surface epithelium (cluster 25) and the rete ovarii (cluster 28). (**E**) Further
1135 analysis of hematopoietic cells using re-clustering in Seurat identified 9 clusters across five
1136 samples. (**F**) The deduced hematopoietic cell subgroups are labeled and indicated by colored
1137 regions, including macrophages (clusters 0, 4, and 7), dendritic cells (cluster 3), neutrophils
1138 (cluster 5), B cells (cluster 1), T cells (cluster 2), NK cells (cluster 6), and mitotic cells (cluster
1139 8). (**G**) Dot plot showing marker gene expression across different hematopoietic cell types.
1140
1141 **Figure supplement 7**. Hormone receptor expression and XO mouse line.
1142 (**A**) Expression levels of hormone receptors (Y-axis) across different cell clusters (X-axis).
1143 Androgen receptor (*Ar*) is expressed in nearly all cell types except hematopoietic cells. (*Esr1*) is
1144 primarily expressed in theca cells, epithelial cells, and smooth muscle cells, whereas estrogen
1145 receptor 2 (*Esr2*) is expressed in granulosa cells as expected. No expression of follicle-
1146 stimulating hormone receptor (*Fshr*) is detected in any cell type, while luteinizing
1147 hormone/choriogonadotropin receptor (*Lhcgr*) is specifically expressed in theca cells.
1148 Progesterone receptor (*Pgr*) is present in smooth muscle cells but absent in granulosa cells. (**B**)
1149 The total follicle count in XO mice at 1 week is significantly lower compared to control XX
1150 mice. Follicle counts were performed using Imaris software on whole-mount stained ovaries. N =
1151 3–5. ** $p < 0.01$. (**C**) By 2 weeks, statistical difference between XO and XX mice were
1152 observed. Follicle counts were performed using Imaris software on whole-mount stained ovaries.
1153 N = 4–5. ** $p < 0.01$; ns, not significant.
1154

Fig. S1

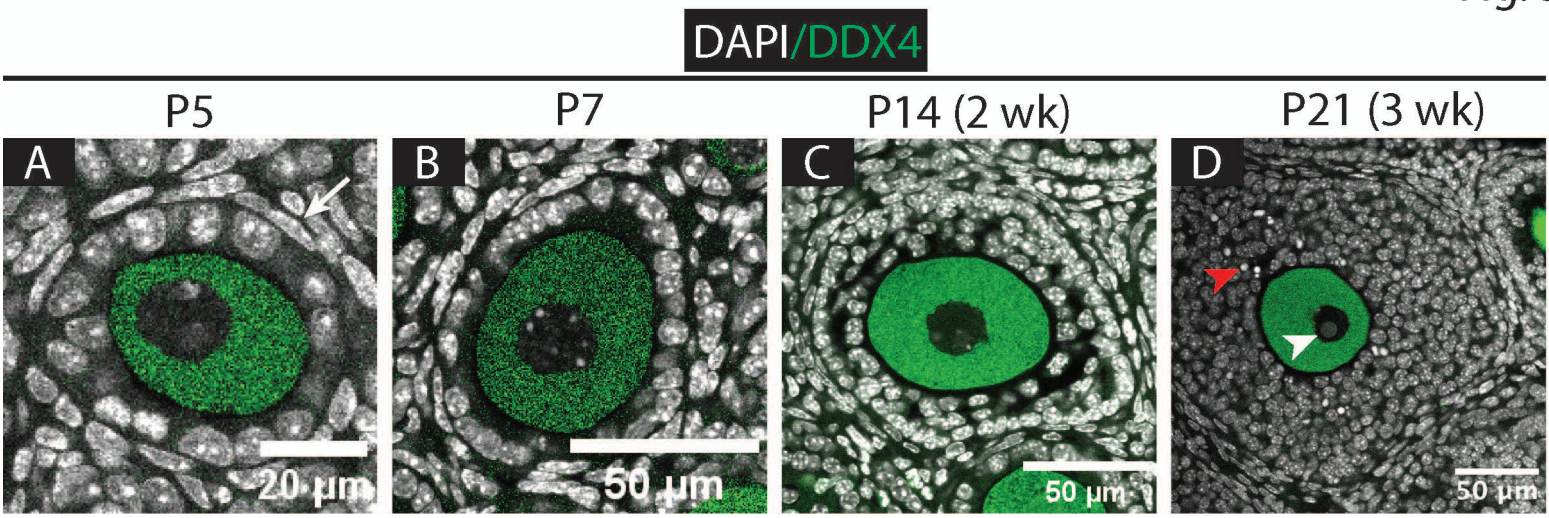

Fig. S2

A

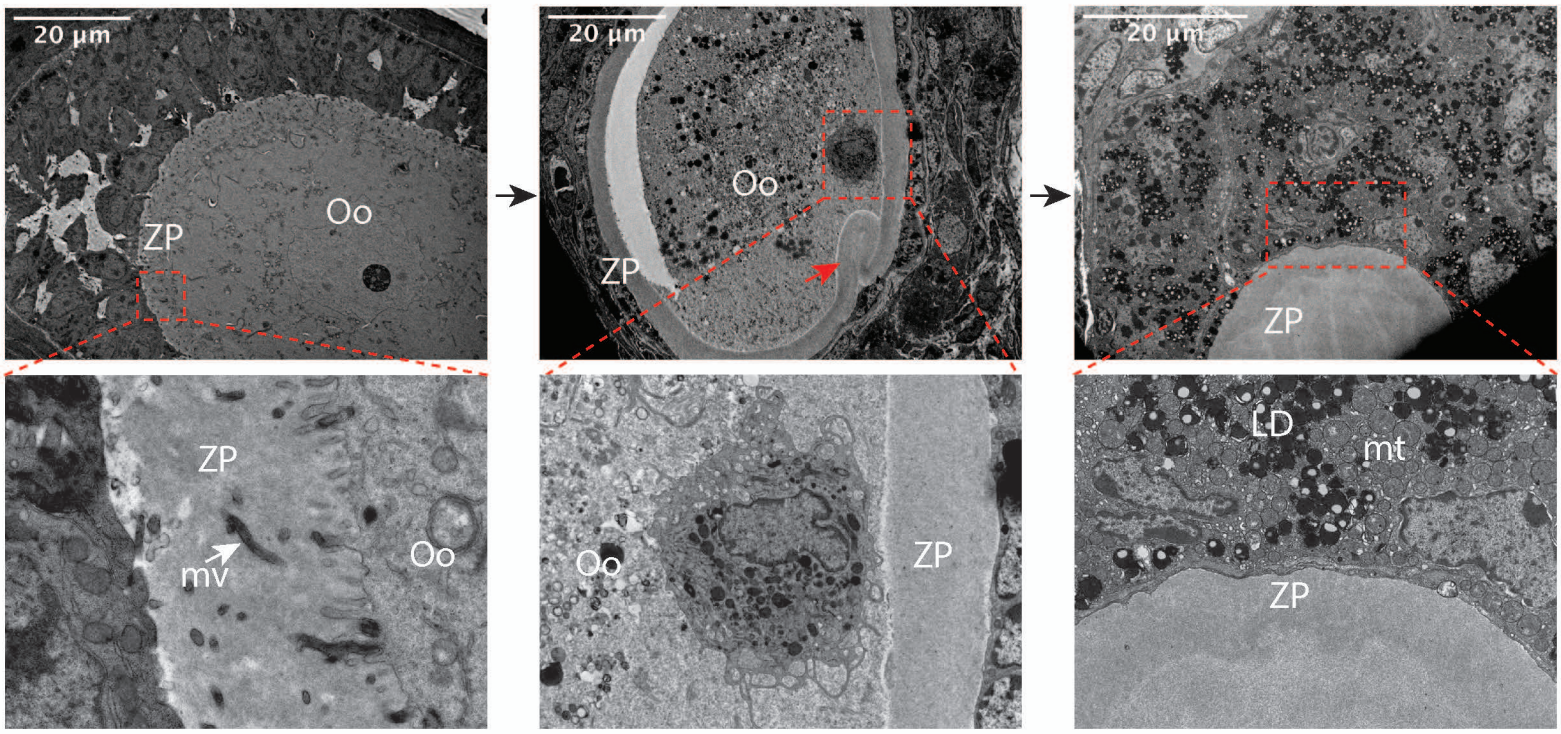

Normal follicle | Intermediate follicle | Atretic follicle

B

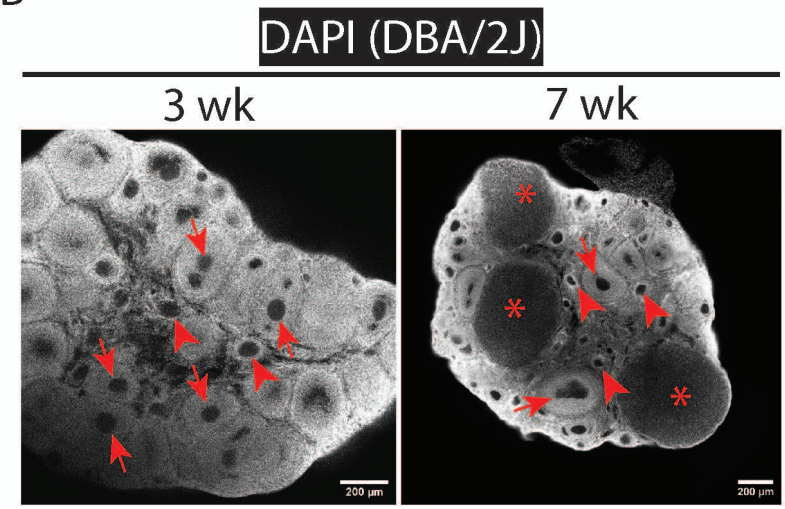

Fig. S3

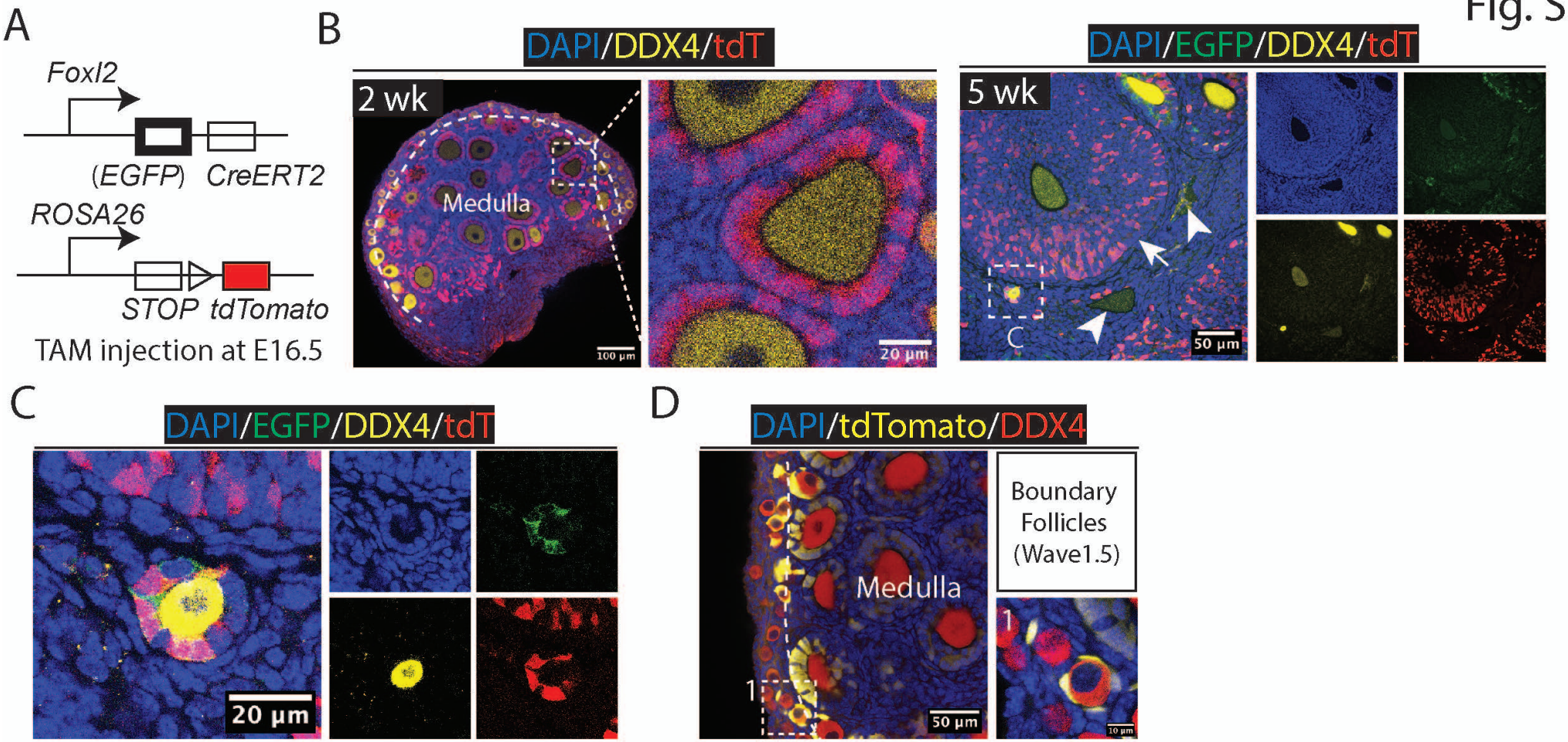
A
Foxl2
(EGFP) CreERT2
ROSA26
STOP tdTomato
TAM injection at E16.5
B
DAPI/DDX4/tdT
2 wk
Medulla
100 µm
20 µm
DAPI/EGFP/DDX4/tdT
5 wk
C
50 µm
C
DAPI/EGFP/DDX4/tdT
20 µm
D
DAPI/tdTomato/DDX4
Medulla
1
50 µm
Boundary Follicles (Wave1.5)
1
10 µm

Fig. S4

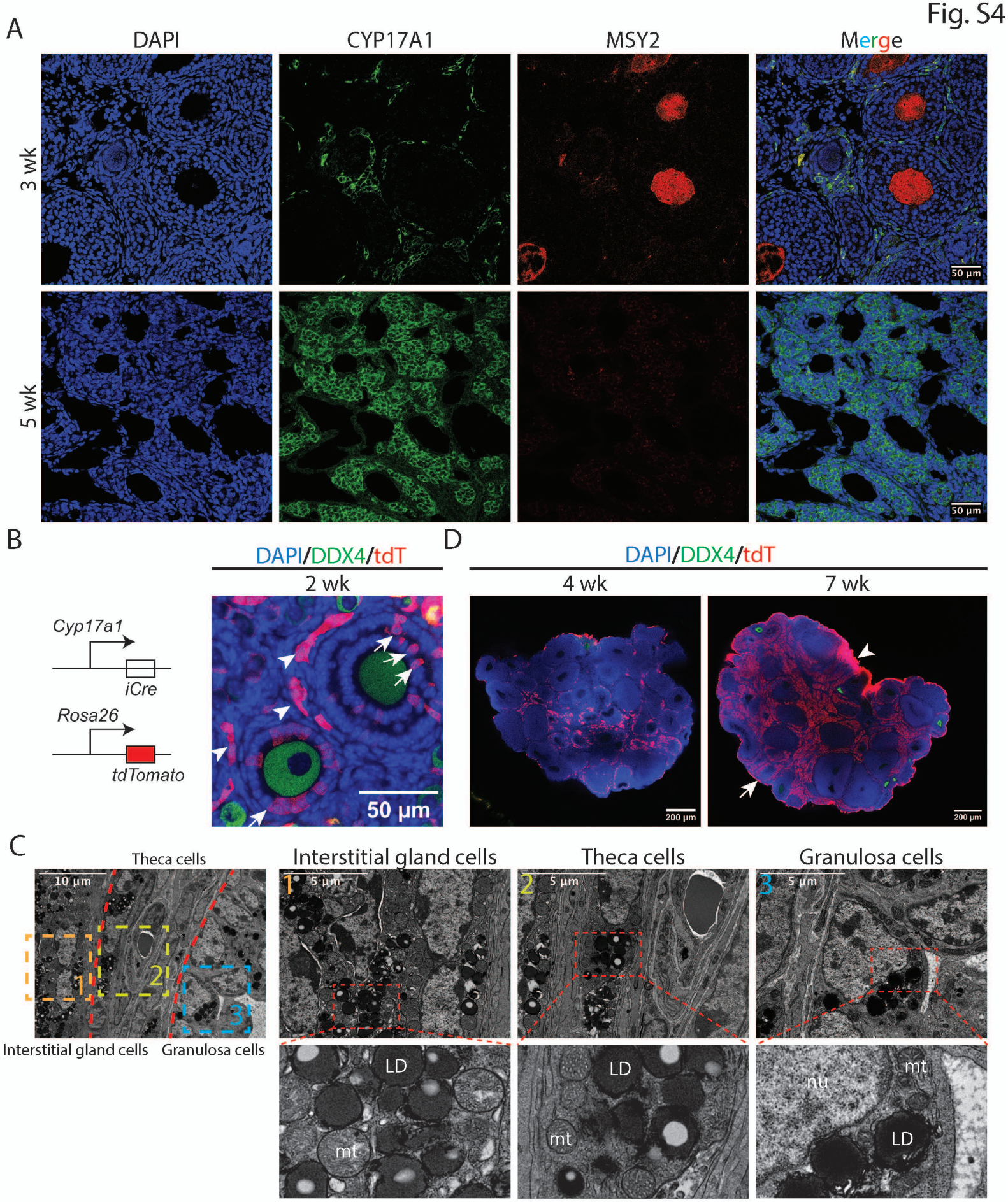
A
DAPI
CYP17A1
MSY2
Merge
3 wk
5 wk
50 µm
B
Cyp17a1
iCre
Rosa26
tdTomato
DAPI/DDX4/tdT
2 wk
50 µm
D
DAPI/DDX4/tdT
4 wk
7 wk
200 µm
C
Theca cells
10 µm
Interstitial gland cells
Granulosa cells
Interstitial gland cells
Theca cells
Granulosa cells
5 µm
LD
mt
nu

Fig. S4

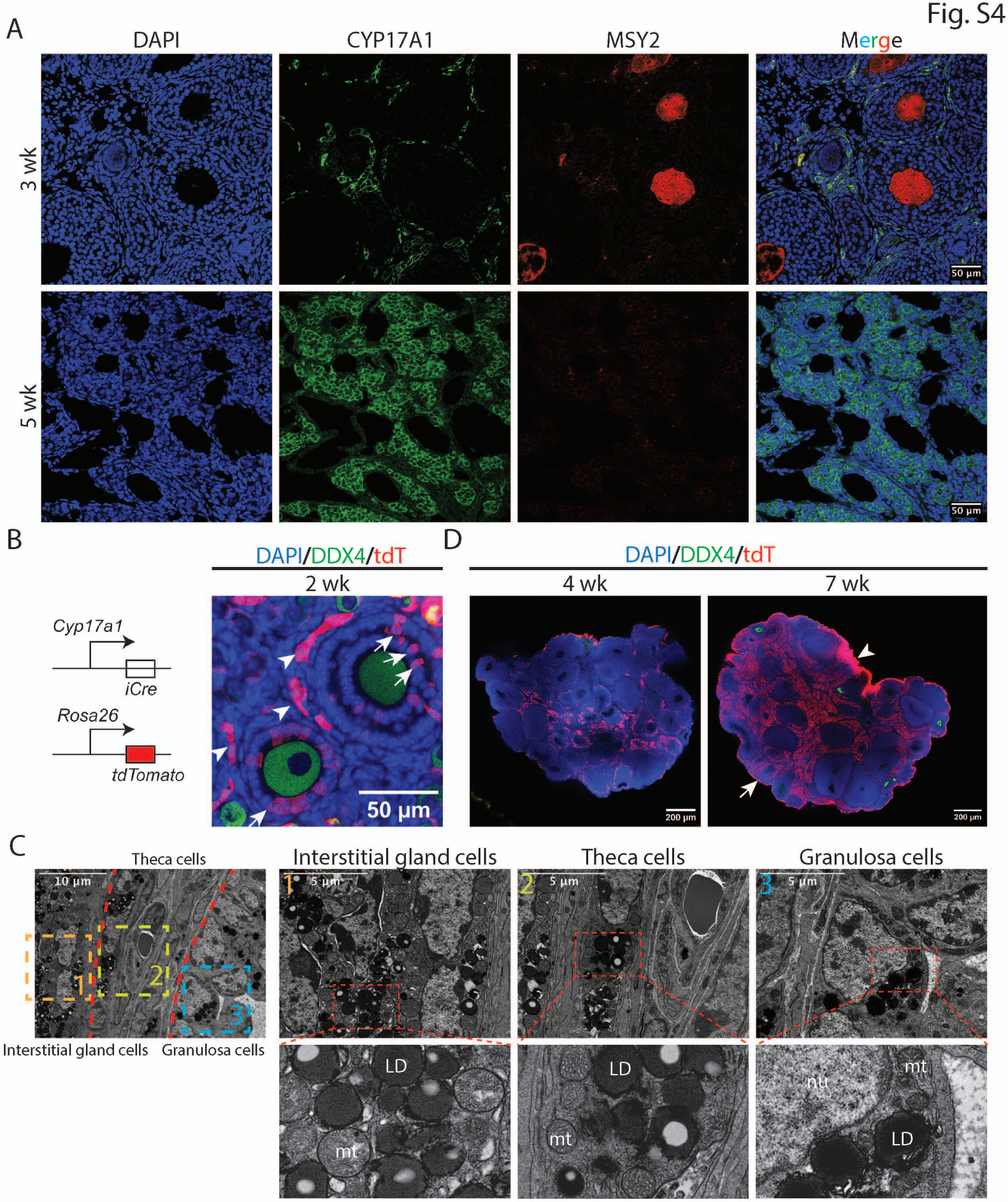
A
DAPI
CYP17A1
MSY2
Merge
3 wk
5 wk
50 µm
B
Cyp17a1
iCre
Rosa26
tdTomato
DAPI/DDX4/tdT
2 wk
50 µm
D
DAPI/DDX4/tdT
4 wk
7 wk
200 µm
C
Theca cells
10 µm
Interstitial gland cells
Granulosa cells
Interstitial gland cells
Theca cells
Granulosa cells
5 µm
LD
mt
nu

Fig. S5

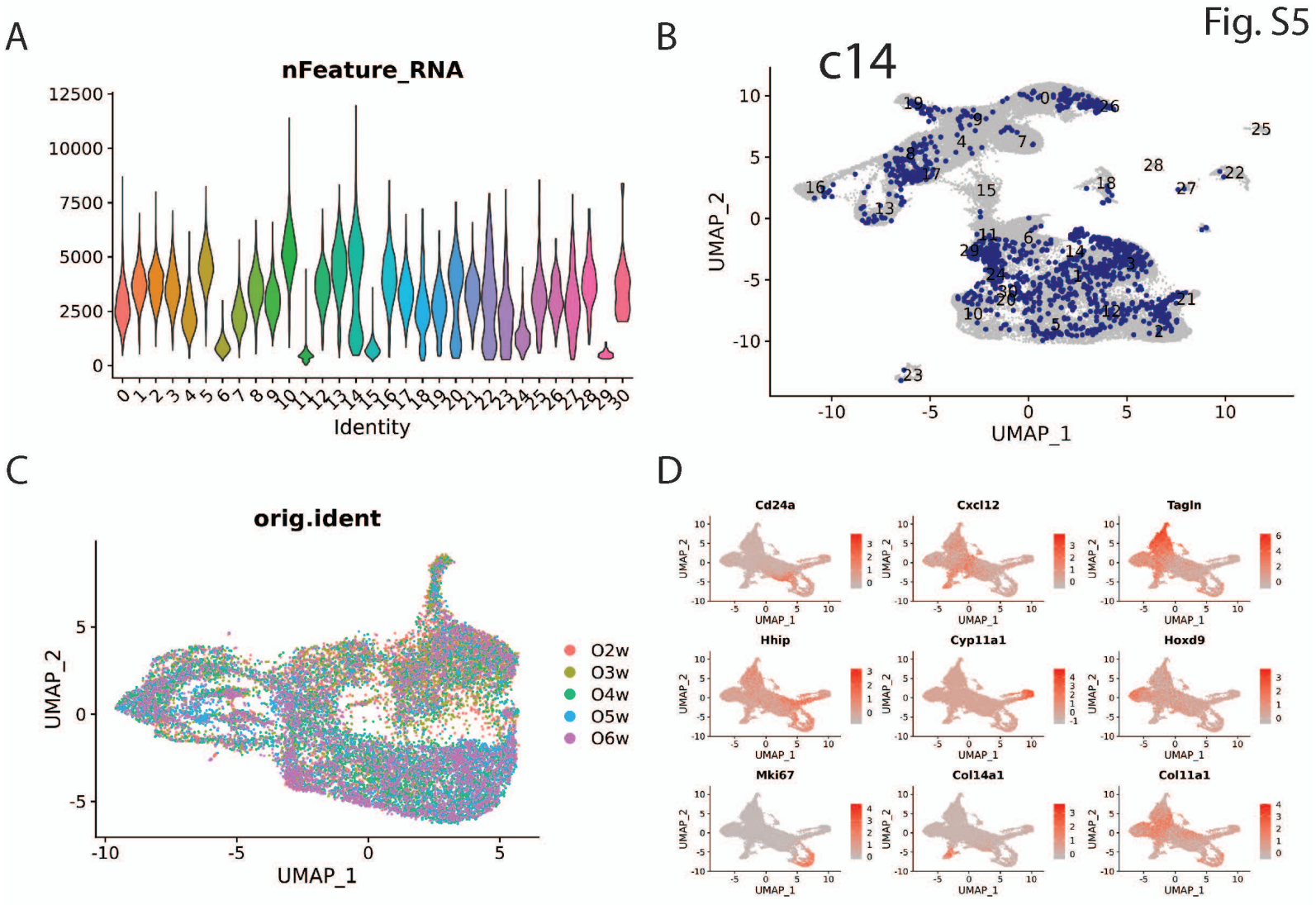
A
nFeature_RNA
Identity
B
c14
UMAP_1
UMAP_2
C
orig.ident
O2w
O3w
O4w
O5w
O6w
UMAP_1
UMAP_2
D
Cd24a
Cxcl12
Tagln
Hhip
Cyp11a1
Hoxd9
Mki67
Col14a1
Col11a1

Fig. S6

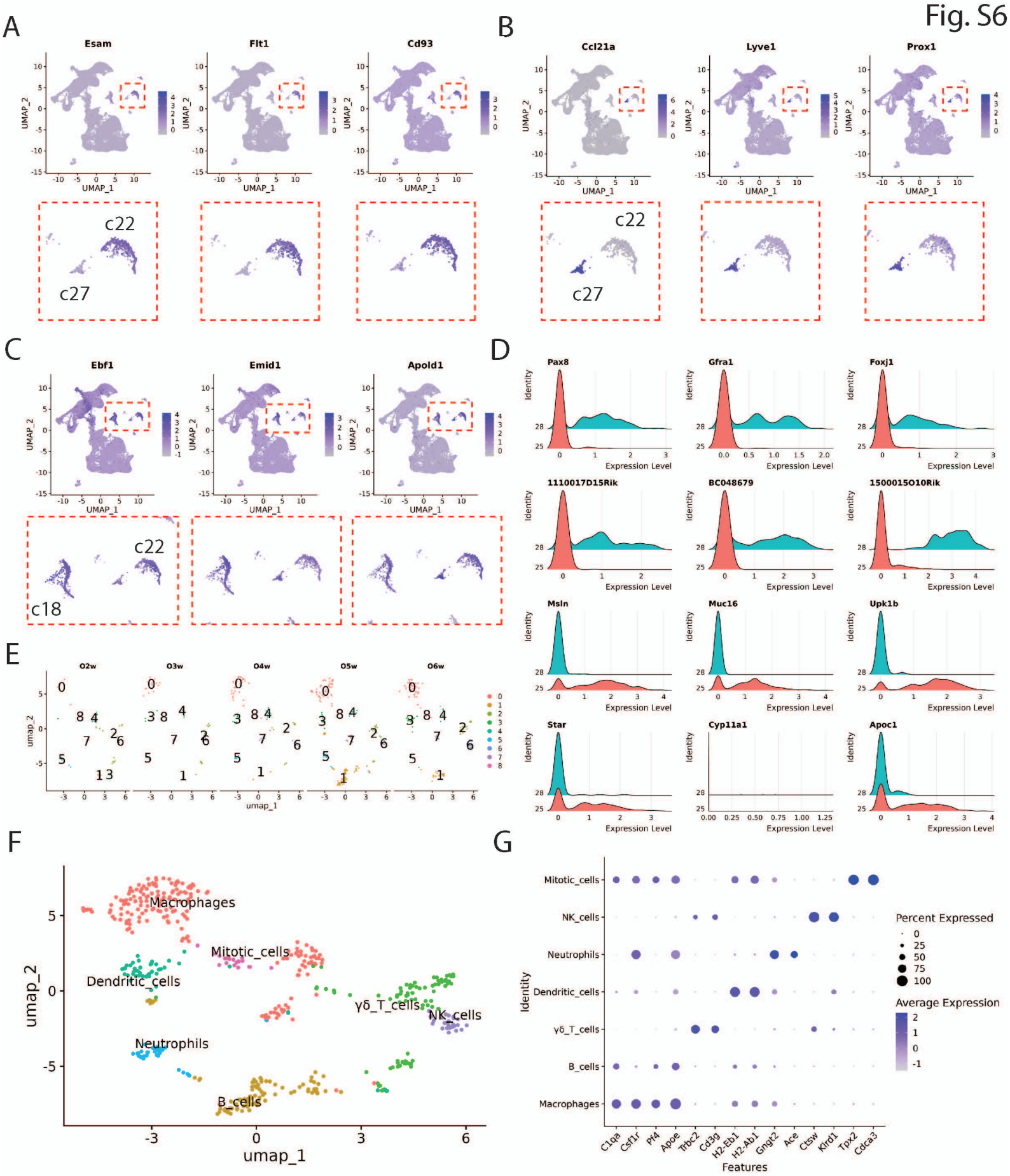
A
Esam
Flt1
Cd93
UMAP_1
UMAP_2
c22
c27
B
Ccl21a
Lyve1
Prox1
c22
c27
C
Ebf1
Emid1
Apold1
c22
c18
D
Pax8
Gfra1
Foxj1
1110017D15Rik
BC048679
1500015O10Rik
Msln
Muc16
Upk1b
Star
Cyp11a1
Apoc1
Identity
Expression Level
E
O2w
O3w
O4w
O5w
O6w
umap_1
umap_2
F
Macrophages
Mitotic_cells
Dendritic_cells
γδ_T_cells
NK_cells
Neutrophils
B_cells
umap_1
umap_2
G
Mitotic_cells
NK_cells
Neutrophils
Dendritic_cells
γδ_T_cells
B_cells
Macrophages
Identity
C1qa
Csf1r
Pf4
Apoe
Trbc2
Cd3g
H2-Eb1
H2-Ab1
Gngt2
Ace
Ctsw
Klrd1
Tpx2
Cdca3
Features
Percent Expressed
0
25
50
75
100
Average Expression
2
1
0
-1

Fig. S7

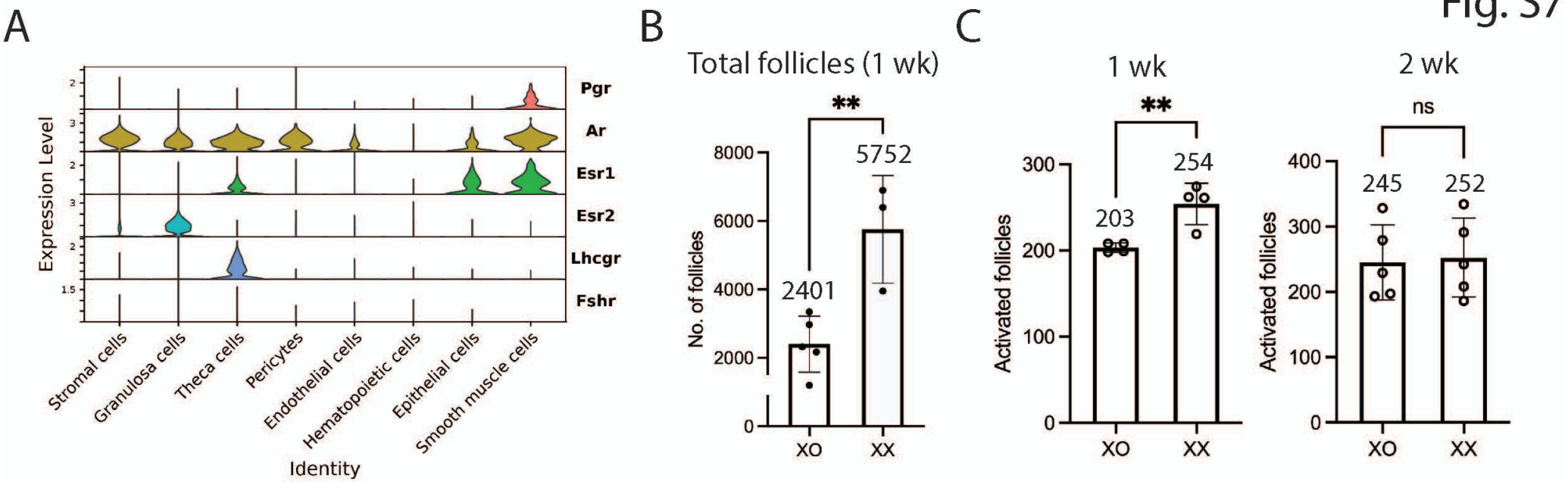
A
Expression Level
Pgr
Ar
Esr1
Esr2
Lhcgr
Fshr
Stromal cells
Granulosa cells
Theca cells
Pericytes
Endothelial cells
Hematopoietic cells
Epithelial cells
Smooth muscle cells
Identity
B
Total follicles (1 wk)
No. of follicles
**
2401
5752
XO
XX
C
1 wk
Activated follicles
**
203
254
XO
XX
2 wk
ns
245
252
XO
XX